

# The SWELL1-LRRC8 complex regulates endothelial AKT-eNOS signaling and vascular function

Ahmad F Alghanem<sup>1,2†</sup>, Javier Abello<sup>3</sup>, Joshua M Maurer<sup>1</sup>, Ashutosh Kumar<sup>1</sup>, Chau My Ta<sup>1</sup>, Susheel K Gunasekar<sup>1</sup>, Urooj Fatima<sup>4</sup>, Chen Kang<sup>1</sup>, Litao Xie<sup>1</sup>, Oluwaseun Adeola<sup>4</sup>, Megan Riker<sup>5</sup>, Macaulay Elliot-Hudson<sup>4</sup>, Rachel A Minerath<sup>4</sup>, Chad E Grueter<sup>4</sup>, Robert F Mullins<sup>5</sup>, Amber N Stratman<sup>3</sup>, Rajan Sah<sup>1,6\*</sup>

<sup>1</sup>Department of Internal Medicine, Cardiovascular Division, Washington University School of Medicine, St. Louis, United States; <sup>2</sup>Eastern Region, King Abdullah International Medical Research Center, King Saud bin Abdulaziz University for Health Sciences, Al Hasa, Saudi Arabia; <sup>3</sup>Department of Cell Biology and Physiology, Washington University in St. Louis, School of Medicine, St. Louis, United States; <sup>4</sup>Department of Internal Medicine, Cardiovascular Division, University of Iowa, Iowa City, United States; <sup>5</sup>Department of Ophthalmology, University of Iowa, Carver College of Medicine, Iowa City, United States; <sup>6</sup>Center for Cardiovascular Research, Washington University, St Louis, United States

\*For correspondence:  
rajan.sah@wustl.edu

Present address: <sup>†</sup>Eastern Region, King Abdullah International Medical Research Center, King Saud bin Abdulaziz University for Health Sciences, Al Hasa, Saudi Arabia

Competing interests: The authors declare that no competing interests exist.

Funding: See page 23

Received: 22 July 2020

Accepted: 22 February 2021

Published: 25 February 2021

Reviewing editor: Mark T Nelson, University of Vermont, United States

© Copyright Alghanem et al. This article is distributed under the terms of the [Creative Commons Attribution License](https://creativecommons.org/licenses/by/4.0/), which permits unrestricted use and redistribution provided that the original author and source are credited.

**Abstract** The endothelium responds to numerous chemical and mechanical factors in regulating vascular tone, blood pressure, and blood flow. The endothelial volume-regulated anion channel (VRAC) has been proposed to be mechanosensitive and thereby sense fluid flow and hydrostatic pressure to regulate vascular function. Here, we show that the leucine-rich repeat-containing protein 8a, LRRC8A (SWELL1), is required for VRAC in human umbilical vein endothelial cells (HUVECs). Endothelial LRRC8A regulates AKT-endothelial nitric oxide synthase (eNOS) signaling under basal, stretch, and shear-flow stimulation, forms a GRB2-Cav1-eNOS signaling complex, and is required for endothelial cell alignment to laminar shear flow. Endothelium-restricted *Lrrc8a* KO mice develop hypertension in response to chronic angiotensin-II infusion and exhibit impaired retinal blood flow with both diffuse and focal blood vessel narrowing in the setting of type 2 diabetes (T2D). These data demonstrate that LRRC8A regulates AKT-eNOS in endothelium and is required for maintaining vascular function, particularly in the setting of T2D.

## Introduction

The endothelium integrates mechanical and chemical stimuli to regulate vascular tone, angiogenesis, blood flow, and blood pressure (Cahill and Redmond, 2016). Endothelial cells express a variety of mechanosensitive and mechanoresponsive ion channels that regulate vascular function (Gerhold and Schwartz, 2016), including TRPV4 (Sonkusare et al., 2012; Earley et al., 2009; Zhang et al., 2009; Mendoza et al., 2010) and Piezo1 (Rode et al., 2017; Li et al., 2014; Coste et al., 2010). The volume-regulated anion channel (VRAC) current is also prominent in endothelium and has been proposed to be mechanoresponsive (Nilius and Droogmans, 2001), to activate in response to fluid flow/hydrostatic pressure (Barakat et al., 1999) and to putatively regulate vascular reactivity. However, the molecular identity of this endothelial ion channel has remained a mystery for nearly two decades.

*Lrrc8a* (leucine-rich repeat-containing protein 8A, also known as SWELL1) encodes a transmembrane protein first described as the site of a balanced translocation in an immunodeficient child with

agammaglobulinemia and absent B-cells (*Sawada et al., 2003; Kubota et al., 2004*). Subsequent work revealed the mechanism for this condition to be due to impaired LRRC8A-dependent GRB2-PI3K-AKT signaling in lymphocytes, resulting in a developmental block in lymphocyte differentiation (*Kumar et al., 2014*). Thus, for ~11 years, LRRC8A was conceived of as a membrane protein that regulates PI3K-AKT mediated lymphocyte function (*Sawada et al., 2003; Kubota et al., 2004*). Although LRRC8A had been predicted to form a hetero-hexameric ion channel complex with other LRRC8 family members (*Abascal and Zardoya, 2012*), it was not until 2014 that LRRC8A was shown to form an essential component of the volume-regulated anion channel (VRAC) (*Qiu et al., 2014; Voss et al., 2014*), forming hetero-hexamers with LRRC8b-e (*Voss et al., 2014; Syeda et al., 2016*). Therefore, historically, LRRC8A was first described as a membrane protein that signaled via protein-protein interactions and then later found to form an ion channel signaling complex.

We showed previously that LRRC8A is an essential component of VRAC in adipocytes (*Zhang et al., 2017*) and skeletal myotubes (*Kumar et al., 2020*), which is required for insulin-PI3K-AKT signaling (*Zhang et al., 2017; Kumar et al., 2020*) to mediate adipocyte hypertrophy (*Zhang et al., 2017*), skeletal myotube differentiation (*Kumar et al., 2020*), skeletal muscle function (*Kumar et al., 2020*), and systemic glucose homeostasis (*Zhang et al., 2017; Kumar et al., 2020; Xie et al., 2017; Gunasekar et al., 2019*). The PI3K-AKT-endothelial nitric oxide synthase (eNOS) signaling pathway is central to transducing both mechanical stretch (*Hu et al., 2013*) and hormonal inputs (insulin) to regulate eNOS expression and activity, which, in turn, regulates vasodilation (blood flow and pressure), inhibits leukocyte aggregation, and limits proliferation of vascular smooth muscle cells (atherosclerosis). Indeed, insulin resistance is thought to be a systemic disorder in the setting of type 2 diabetes (T2D), affecting endothelium in addition to traditional metabolically important tissues, such as adipose, liver, and skeletal muscle (*Janus et al., 2016; Kearney et al., 2008; Muniyappa and Sowers, 2013*). In fact, insulin-resistant endothelium and the resultant impairment in PI3K-AKT-eNOS signaling have been proposed to underlie much of the endothelial dysfunction observed in the setting of obesity and T2D, predisposing to hypertension, atherosclerosis, and vascular disease (*Janus et al., 2016; Kearney et al., 2008; Muniyappa and Sowers, 2013*).

In this study, we demonstrate that VRAC is LRRC8A-dependent in endothelium, associates with GRB2, caveolin-1 (Cav1), eNOS, and regulates PI3K-AKT-eNOS signaling and flow-mediated endothelial cell orientation – suggesting that LRRC8 channel complexes link insulin and mechano-signaling in endothelium. LRRC8A-dependent AKT-eNOS, ERK1/2, and mTOR signaling influences blood pressure and vascular function in vivo, while impaired endothelial LRRC8A signaling predisposes to vascular dysfunction in the setting of diet-induced T2D.

## Results

### ***Lrrc8a* functionally encodes VRAC current in endothelium**

The volume-regulatory anion channel (VRAC) current has been measured and characterized in endothelial cells for decades but the molecular identity of this endothelial ion channel remains elusive (*Nilius and Droogmans, 2001; Barakat et al., 1999; Barakat, 1999*). To determine if the leucine-rich repeat-containing membrane protein LRRC8A recently identified in cell lines (*Qiu et al., 2014; Voss et al., 2014*) is required for VRAC in endothelial cells, as it is in adipocytes (*Zhang et al., 2017*), skeletal myoblasts (*Kumar et al., 2020*) pancreatic  $\beta$ -cells (*Kang et al., 2018; Stuhlmann et al., 2018*), nodose neurons (*Wang et al., 2017*), and spermatozoa (*Lück et al., 2018*), we first confirmed robust LRRC8A protein expression by Western blot (**Figure 1A**) and immunostaining (**Figure 1B**) in human umbilical vein endothelial cells (HUVECs). LRRC8A protein expression is substantially reduced upon adenoviral transduction with a short-hairpin RNA directed to *Lrrc8a* (Ad-sh*Lrrc8a*-mCherry) as compared to a scrambled control (Ad-sh*Scr*-mCherry). Next, we measured hypotonically induced (210 mOsm) endothelial VRAC currents in HUVECs. These classic outwardly rectifying hypotonically induced VRAC currents are prominent in HUVECs, largely blocked by the VRAC current inhibitor 4-(2-butyl-6,7-dichloro-2-cyclopentyl-indan-1-on-5-yl) oxobutyric acid (DCPIB; **Figure 1C&D**), and significantly suppressed upon sh*Lrrc8a*-mediated LRRC8A knock-down (KD) (**Figure 1E&F**), consistent with LRRC8A functionally encoding endothelial VRAC.

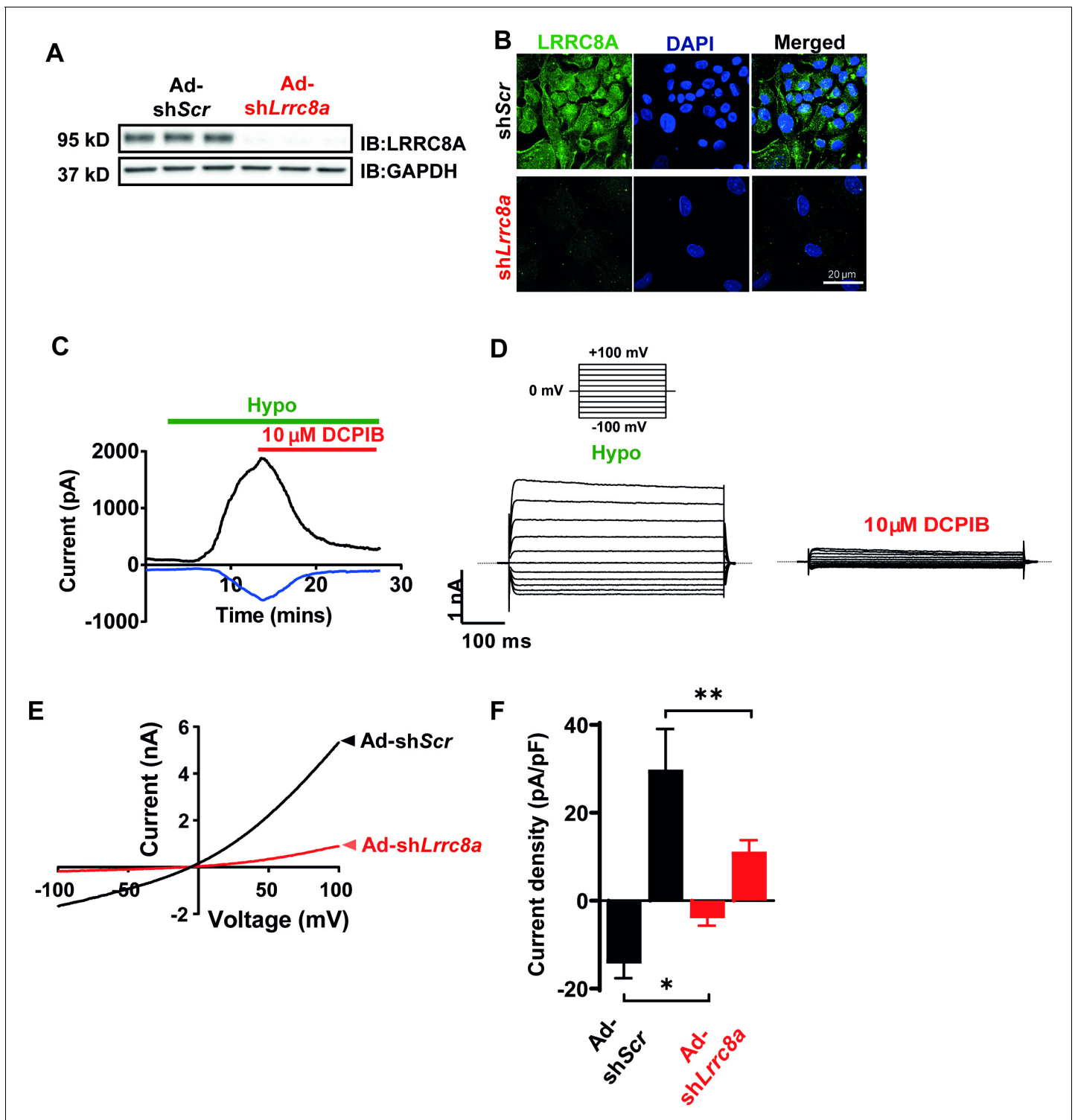


**Figure 1.** Leucine-rich repeat-containing protein 8a (LRRRC8A) mediates volume-regulated anion channel (VRAC) currents in human umbilical vein endothelial cells (HUVECs). (A) LRRRC8A Western blot in HUVECs transduced with adenovirus expressing a short-hairpin RNA directed to LRRRC8A (Ad-shLrrc8a) compared to control scrambled short-hairpin RNA (Ad-shScr). GAPDH is used as loading control. (B) Immunofluorescence staining of the HUVECs transduced with Ad-shLrrc8a and Ad-shScr. (C) Current-time relationship of VRAC current (hypotonic, 210 mOsm) in Ad-shScr transduced HUVEC and co-application of 10  $\mu$ M 4-(2-butyl-6,7-dichloro-2-cyclopentyl-indan-1-on-5-yl) oxobutyric acid (DCPIB). (D) Representative current traces upon hypotonic activation (left) during voltage steps (from -100 to +100 mV, shown in inset) and inhibition by DCPIB (right). (E) Current-voltage relationship of VRAC during voltage ramps from -100 mV to +100 mV after hypotonic swelling in HUVECs transduced with Ad-shScr and Ad-shLrrc8a. *Figure 1 continued on next page*

Figure 1 continued

(F) Mean current outward and inward densities at +100 and -100 mV ( $n_{shSCR}=4$  cells;  $n_{shLrrc8a}=6$  cells). Data are shown as mean  $\pm$  s.e.m. \* $p<0.05$ ; \*\* $p<0.01$ ; unpaired t-test for (F).

The online version of this article includes the following source data for figure 1:

**Source data 1.** Source data for **Figure 1F**.

## LRRC8A regulates PI3K-AKT-eNOS, ERK, and mTOR signaling in endothelium

Previous studies in adipocytes (Zhang et al., 2017) and skeletal muscle (Kumar et al., 2020) demonstrate that LRRC8A regulates insulin-PI3K-AKT signaling (Zhang et al., 2017; Kumar et al., 2020), adipocyte expansion (Zhang et al., 2017), skeletal muscle function (Kumar et al., 2020), and systemic glycemia, whereby LRRC8A loss-of-function induces an insulin-resistant pre-diabetic state (Zhang et al., 2017; Kumar et al., 2020; Xie et al., 2017). Insulin signaling is also important in regulating endothelium and vascular function (Kearney et al., 2008; Muniyappa and Sowers, 2013; Duncan et al., 2008). Moreover, insulin resistance in T2D is considered a systemic disorder and insulin-resistant endothelium is postulated to underlie impaired vascular function in T2D (Kearney et al., 2008; Muniyappa and Sowers, 2013). As LRRC8A is highly expressed in endothelium (Figure 1) and PI3K-AKT-eNOS signaling is critical for endothelium-dependent vascular function (Morello et al., 2009), we next examined AKT-eNOS, ERK1/2, and mTOR signaling in LRRC8A KD compared to control HUVECs under basal conditions. Basal phosphorylated AKT2 (pAKT2, Figure 2A&D), pAKT1 (Figure 2A&E), phosphorylated eNOS (p-eNOS) (Figure 2A&C), and pERK1/2 (Figure 2A&F) are abrogated in HUVECs upon LRRC8A KD, indicating that LRRC8A contributes to AKT-eNOS and ERK signaling in endothelium. Curiously, basal pS6 ribosomal protein, indicative of mTOR signaling, is augmented in LRRC8A KD HUVECs compared to control (Figure 2A&G), suggesting LRRC8A to be a negative regulator of mTOR in endothelium. As a complementary approach, we used siRNA mediated LRRC8A KD using a silencer select siRNA targeting *Lrrc8a* mRNA with a different sequence from *shLrrc8a*. siRNA mediated LRRC8A KD in HUVECs yielded nearly identical results to the shRNA KD approach (Figure 2—figure supplement 1). In summary, LRRC8A expression level regulates AKT, eNOS, ERK, and mTOR signaling in endothelium.

## LRRC8A interacts with GRB2, Cav1, and eNOS and mediates stretch-dependent eNOS signaling

In adipocytes, the mechanism of LRRC8A-mediated regulation of PI3K-AKT signaling involves LRRC8A/GRB2/Cav1 molecular interactions (Zhang et al., 2017). To determine if LRRC8A resides in a similar macromolecular signaling complex in endothelium, we immunoprecipitated (IP) endogenous GRB2 from HUVECs. Upon GRB2 IP, we detected LRRC8A protein in *shScr*-treated HUVECs and less LRRC8A upon GRB2 IP from *shLrrc8a*-treated HUVECs, consistent with an LRRC8A-GRB2 interaction (Figure 3A&B). In addition, with GRB2 IP, we also detected both Cav1 (Figure 3A&B) and eNOS (Figure 3B). These data suggest that endothelial LRRC8A resides in a signaling complex that includes GRB2, Cav1, and eNOS, consistent with the findings that GRB2 and Cav1 interact, and that Cav1 regulates eNOS via a direct interaction (Ju et al., 1997; Venema et al., 1997; Goligorsky et al., 2002). Also, GRB2 has been shown to regulate endothelial ERK, AKT, and JNK signaling (Salameh et al., 2005). Moreover, these data are also in line with the notion that caveoli form mechanosensitive microdomains (Nassey and Lamaze, 2012; Sinha et al., 2011; Sedding et al., 2005) which regulate VRAC (Trouet et al., 2001; Trouet et al., 1999; Egorov et al., 2019), and VRAC can be activated by mechanical stimuli in a number of cell types, including endothelium (Nilius and Droogmans, 2001; Barakat, 1999; Browe and Baumgarten, 2003; Browe and Baumgarten, 2006; Nakao et al., 1999; Romanenko et al., 2002).

We also examined the relationship between LRRC8A and eNOS protein expression and localization in HUVECs by immunofluorescence (IF) staining (Figure 3C). Similar to observed by Western blot (Figure 2A, Figure 2—figure supplement 1), IF staining revealed that reductions in LRRC8A expression correlate with reduced eNOS expression (Figure 3C–E, Figure 3—figure supplement 1). Moreover, LRRC8A and eNOS co-localization in plasma membrane and perinuclear intracellular domains (Figure 3C, inset) were consistent with the IP data, revealing an LRRC8A-GRB2-Cav-eNOS

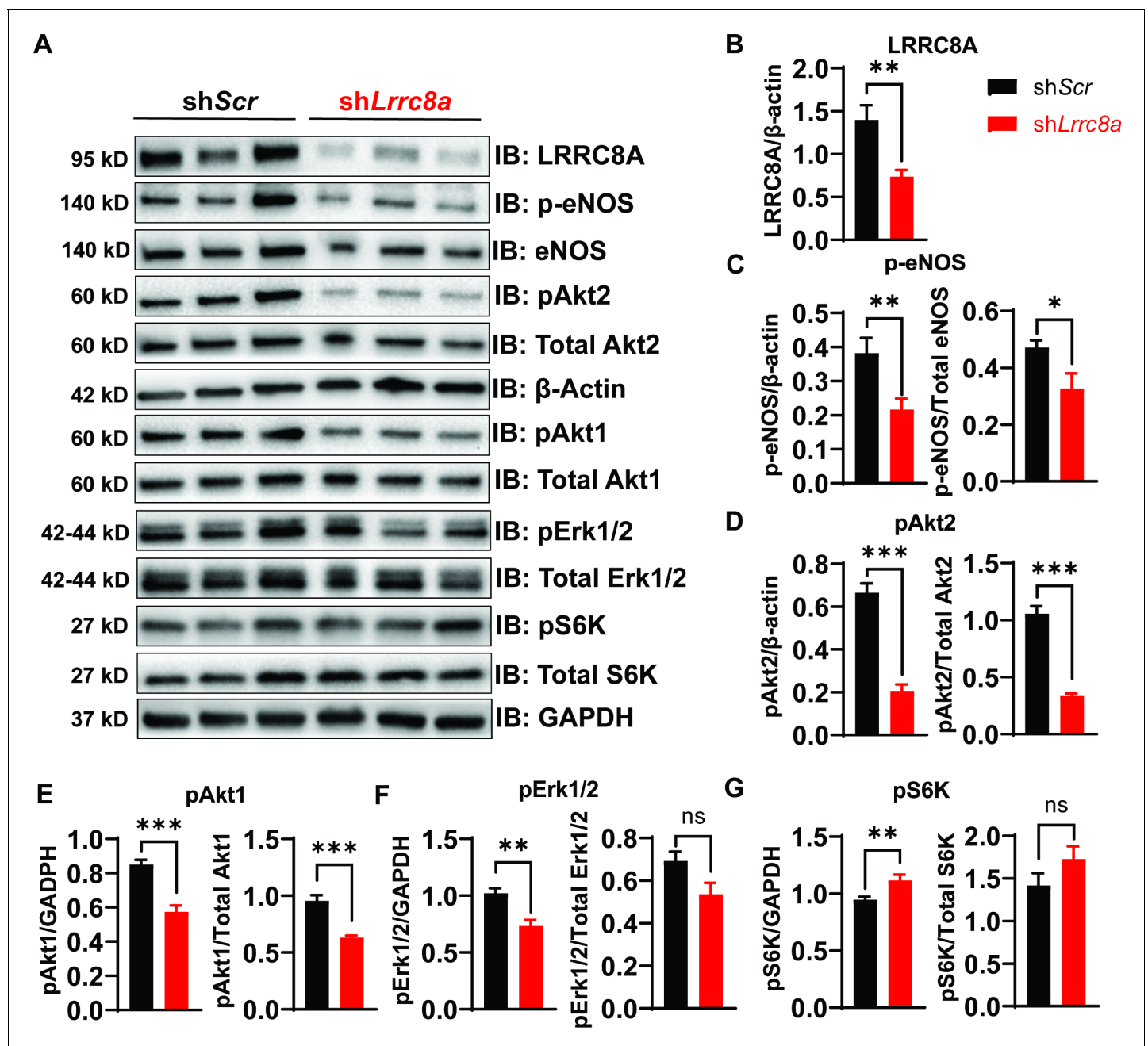


**Figure 2.** Leucine-rich repeat-containing protein 8a (LRRC8A) regulates PI3K-AKT-endothelial nitric oxide synthase (eNOS), ERK signaling in endothelium. (A) Western blots of LRRC8A, pAkt2, pAkt1, Akt2, Akt1, pErk1/2, Erk1/2, phosphorylated eNOS (p-eNOS), eNOS, pS6K ribosomal protein, S6K ribosomal protein, GAPDH, and β-actin in Ad-shScr and Ad-shLrrc8a transduced human umbilical vein endothelial cells (HUVECs) under basal conditions. Quantification of LRRC8A/β-actin (B), p-eNOS/β-actin, p-eNOS/total eNOS (C), pAkt2/β-actin, pAkt2/total Akt2 (D), pAkt1/GAPDH, pAkt1/total Akt1 (E), pERK1/2/GAPDH, pErk1/2/total Erk1/2 (F), pS6K ribosomal protein/GAPDH, and pS6K ribosomal protein/total S6K ribosomal protein (G). N = 6 independent experiments. Significance between the indicated groups in all blots was calculated using a two-tailed unpaired Student's t-test. Data are shown as mean ± s.e.m. \*p<0.05; \*\*p<0.01; \*\*\*p<0.001.

The online version of this article includes the following source data and figure supplement(s) for figure 2:

**Source data 1.** Source data for **Figure 2**.

**Figure supplement 1.** Leucine-rich repeat-containing protein 8a (LRRC8A) regulates PI3K-AKT-endothelial nitric oxide synthase (eNOS) and ERK signaling in endothelium.

**Figure supplement 1—source data 1.** Source data for **Figure 2—figure supplement 1**.

interaction (**Figure 3A&B**), and also with the previously described intracellular eNOS localization (**Fulton et al., 2002**).

Given that endothelial cells respond to stretch stimuli to regulate vascular tone via activation of eNOS (**Jufri et al., 2015**), we next examined the LRRC8A dependence of stretch-induced AKT, ERK1/2, and eNOS signaling in HUVECs (**Figure 4**), similar to several previous studies (**Hsu et al., 2010; Shi et al., 2007; Liu et al., 2003; Goettsch et al., 2009**). Stretch (5%) was sufficient to stimulate AKT1 and AKT2 signaling (**Figure 4A–C**), though not ERK1/2 signaling (**Figure 4D**) in HUVECs, and all were blunted in LRRC8A KD HUVECS (**Figure 4A–D**). Similarly, we observed abrogation of time-dependent p-eNOS signaling with 5% stretch in LRRC8A KD HUVECs compared to control (**Figure 4E&F**). Taken together, these data position LRRC8A as a regulator stretch-mediated PI3K-AKT-eNOS signaling in endothelium.

## Endothelial cell orientation to the direction of shear flow is impaired upon LRRC8A KD

To evaluate the requirement of LRRC8A for endothelial cell responses to physiological mechanical stimuli relevant to endothelium, we examined the LRRC8A dependence of HUVEC orientation to laminar shear flow. In response to laminar shear flow at 15 dynes/cm<sup>2</sup> for 24 hr (**Figure 5A**), siControl transfected HUVECs oriented well to the direction of flow (**Figure 5B–F** and **Figure 5—videos 1** and **2**), while LRRC8A KD HUVEC exhibited impaired flow-mediated alignment (**Figure 5B–F** and **Figure 5—videos 3** and **4**). These LRRC8A-dependent differences were also apparent in the degree of impairment of HUVEC elongation to the direction of fluid flow (**Figure 5G**) and in the velocity of movement against the direction of flow (**Figure 5H&I**).

Next, we asked whether shear-flow-mediated eNOS phosphorylation is LRRC8A-dependent, as observed with stretch-mediated signaling (**Figure 4**). We stimulated siScr and siLrrc8a transfected HUVECs with either no flow, or laminar shear flow for 2 or 24 hr and then immunostained for p-eNOS (**Figure 5J**). We observed marked p-eNOS induction in response to shear flow after both 2 and 24 hr in siControl transfected HUVECs, and this was significantly abrogated upon LRRC8A KD (**Figure 5J**). Interestingly, this shear-flow stimulated p-eNOS displayed significant nuclear localization, consistent with prior reports (**Feng et al., 1999; Andersson and Brittebo, 2012; Wang et al., 2019; Gobeil et al., 2006**). The same nuclear distribution was also observed using a different p-eNOS antibody (**Figure 5—figure supplement 1**). We quantified the intensity of p-eNOS staining in two ways: p-eNOS excluding the nuclear signal (**Figure 5K,L**) and p-eNOS in the entire cell (**Figure 5M,O**). In both cases, we observed significant shear-flow-mediated p-eNOS induction in siScr HUVECs, after both 2 hr and 24 hr flow, and this was reduced in LRRC8A KD HUVEC (**Figure 5K–O**), consistent with LRRC8A-dependent flow-mediated p-eNOS signaling.

## Genome-wide mRNA profiling reveals LRRC8A-dependent regulation of multiple processes involved in angiogenesis, atherosclerosis, and vascular function

Genome-wide transcriptome analysis of LRRC8A KD HUVEC compared to control (RNA sequencing) revealed multiple pathways enriched regulating angiogenesis, migration, and tumorigenesis, including GADD45, IL-8, p70S6K (mTOR), TREM1, angiopoietin, and HGF signaling (**Figure 6, Supplementary file 1** and **2**). Pathways linked to cell adhesion and renin-angiotensin signaling are also enriched – both pathways and processes that are known to be altered in vasculature in the setting of atherosclerosis and T2D. Also, notable are statistically significant increases in VEGFA (1.6-fold) and CD31 (2.0-fold) expression in LRRC8A KD HUVECs (**Figure 6C**), both of which are pro-angiogenic and associated with mTORC1 hyperactivation (**Ding et al., 2018**). CD36 is increased 3.4-fold and is also pro-angiogenic (**Silverstein and Febbraio, 2009**) and pro-atherosclerotic (**Park, 2014; Harb et al., 2009; Kennedy et al., 2009**). Moreover, the trends toward reduced eNOS protein expression observed upon LRRC8A KD in HUVECs (**Figure 2A, Figure 2—figure supplement 1, Figure 3C&E, Figure 3—figure supplement 1**) are also associated with twofold reduced eNOS mRNA expression (NOS3, **Figure 6C**). Notably, *Lrrc8a* mRNA expression in HUVECs is higher than many classical endothelial markers expressed in endothelium (EPOR, CDH5, CD36, VWF, PECAM1, KDR, VEGFA, **Figure 6C**). HUVEC *Lrrc8a* mRNA expression is also 2.5-fold higher than Piezo1 (**Figure 6C**), a mechanosensitive ion channel (**Coste et al., 2010; Coste et al., 2012**) with a

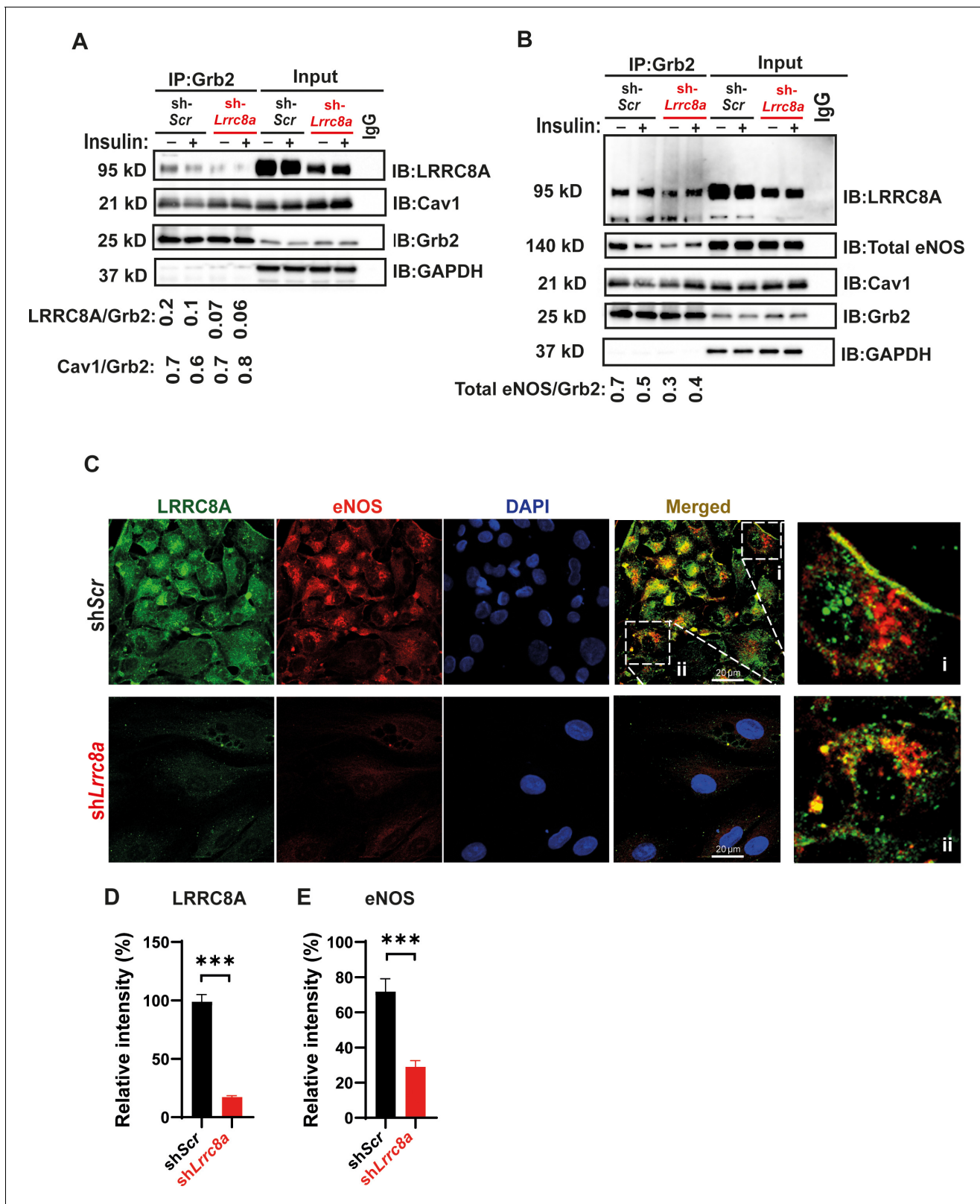


**Figure 3.** Leucine-rich repeat-containing protein 8A (LRRC8A) interacts with Grb2, Cav1, and endothelial nitric oxide synthase (eNOS) in human endothelium. (A) GRB2 immunoprecipitation from Ad-shScr and Ad-shLrrc8a transduced human umbilical vein endothelial cells (HUVECs) and immunoblot with LRRC8A, Cav1, and GRB2 antibodies. Densitometry values for GRB2 co-immunoprecipitated LRRC8A (LRRC8A/GRB2) and GRB2 co-immunoprecipitated Cav1 (Cav1/GRB2). GAPDH serves as loading control for input samples. (B) GRB2 immunoprecipitation from Ad-shScr and Ad-shLrrc8a transduced HUVECs and immunoblot with LRRC8A, Total eNOS, Cav1, and GRB2 antibodies. Densitometry values for Total eNOS co-immunoprecipitated GRB2 (Total eNOS/GRB2). GAPDH serves as loading control for input samples. (C) Immunofluorescence images of HUVECs transduced with Ad-shScr (shScr) or Ad-shLrrc8a (shLrrc8a) stained for LRRC8A (green), eNOS (red), and DAPI (blue). Scale bars, 20  $\mu$ m. (D) Quantification of LRRC8A relative intensity in shScr and shLrrc8a cells. (E) Quantification of eNOS relative intensity in shScr and shLrrc8a cells. \*\*\*p < 0.001. Figure 3 continued on next page

Figure 3 continued

sh*Lrrc8a* transduced HUVECs and immunoblot with LRRC8A, eNOS, Cav1, and GRB2 antibodies. Insulin stimulation: 100 nM insulin for 10 min. Densitometry values for GRB2 co-immunoprecipitated eNOS (eNOS/GRB2). Representative blots from three independent experiments. (C) Representative endogenous LRRC8A and eNOS immunofluorescence staining in Ad-sh*Scr* and Ad-sh*Lrrc8a* transduced HUVECs. Representative image from six independent experiments. (D–E) Quantification of LRRC8A (D, n = 6) and eNOS (E, n = 6) immunofluorescence staining upon LRRC8A knock-down (KD). Evidence of LRRC8A-eNOS co-localization (C, insets) in plasma membrane (i) and perinuclear regions (ii). Significance between the indicated groups is calculated using an unpaired two-tailed Student's t-test. p-Values are indicated on figures. Data are shown as mean ± s.e.m. \*\*\*p<0.001. The online version of this article includes the following source data and figure supplement(s) for figure 3:

**Source data 1.** Source data for **Figure 3D**.

**Source data 2.** Source data for **Figure 3E**.

**Figure supplement 1.** Leucine-rich repeat-containing protein 8a (LRRC8A) co-localizes with endothelial nitric oxide synthase (eNOS) and regulates eNOS expression.

well-established role in endothelial biology and vascular function (Rode et al., 2017; Li et al., 2014), and Piezo1 mRNA expression does not change upon LRRC8A KD. Also, *Lrrc8a* mRNA expression is the highest among all *LRRC8* genes expressed in HUVECs, 3-fold higher than *Lrrc8a* mRNA in 3T3-F442A adipocytes (Zhang et al., 2017), 15-fold higher than C2C12 myotubes (Kumar et al., 2020; Figure 6D), consistent with the prominent endogenous  $I_{Cl,SWELL}$  currents present in HUVEC (Figure 1C–F).

### Endothelial-targeted LRRC8A KO mice exhibit mild angiotensin-II stimulated hypertension and impaired retinal blood flow in the setting of T2D

To examine the functional consequences of endothelial LRRC8A ablation in vivo, we generated endothelial-targeted *Lrrc8a* knock-out mice (e*Lrrc8a* KO) by crossing *Lrrc8a* floxed mice (Zhang et al., 2017; Kumar et al., 2020; Kang et al., 2018) with the endothelium-restricted CDH5-Cre mouse (CDH5-Cre; *Lrrc8a*<sup>fl/fl</sup>; Figure 7A). Patch-clamp recordings of primary endothelial cells isolated from WT and e*Lrrc8a* KO mice (Figure 7B) reveal robust hypotonically activated currents (Hypo, 210 mOsm) in WT endothelial cells, which are DCPIB inhibited (Figure 7C&E), while e*Lrrc8a* KO endothelial cells exhibit markedly reduced hypotonically activated currents (Figure 7D&E). Consistent with this, IF staining of aortic ring explants from WT and e*Lrrc8a* KO mice confirmed LRRC8A ablation from CD31+ primary endothelial cells (Figure 7F&G).

Based on our findings that LRRC8A regulates AKT-eNOS signaling in HUVECs in vitro, we next examined p-eNOS in aortic endothelium by IF staining in WT and LRRC8A KO mice. Similar to results in LRRC8A KD HUVEC, we found reduced p-eNOS intensity in aortic endothelium of e*Lrrc8a* KO mice as compared to WT mice (Figure 7H,I).

Since eNOS signaling is central to blood pressure regulation, we next examined blood pressures in e*Lrrc8a* KO mice compared to WT controls (*Lrrc8a*<sup>fl/fl</sup> mice). Male mice exhibited no significant differences in systolic blood pressure under basal conditions (Figure 7J), while female mice were mildly hypertensive relative to WT mice (Figure 7K). However, after 4 weeks of angiotensin-II (Ang II) infusion, male e*Lrrc8a* KO mice developed exacerbated systolic hypertension as compared to Ang II-treated WT mice (Figure 7L). These data are consistent with endothelial dysfunction and impaired vascular relaxation in e*Lrrc8a* KO mice, resulting in a propensity for systolic hypertension.

As endothelial dysfunction may also result in impaired blood flow, we performed retinal imaging during intraperitoneal (i.p.) injection of fluorescein to assess retinal vessel blood flow and morphology in WT and e*Lrrc8a* KO mice. Mice raised on a regular diet had mild, non-significant impairments in retinal blood flow, based on the relative rate of rise of the fluorescein signal in retinal vessels (Figure 8—figure supplement 1). There was evidence of mild focal narrowing of retinal vessels in e*Lrrc8a* KO as compared to WT mice (Figure 8—figure supplement 1A,D&E), with no significant differences in other parameters (Figure 8—figure supplement 1F–K). In mice raised on high-fat high-sucrose (HFHS) diet, retinal blood flow was more severely impaired (Figure 8A–C) with significant focal and diffuse retinal vessel narrowing in e*Lrrc8a* KO mice compared to WT mice (Figure 8A, F–H, Figure 8—figure supplement 2, Figure 8—video 1), and this relative difference was markedly worse in female compared to male mice. These findings are all consistent with endothelial dysfunction and impaired retinal vessel vasorelaxation due to reduced eNOS expression and activity,

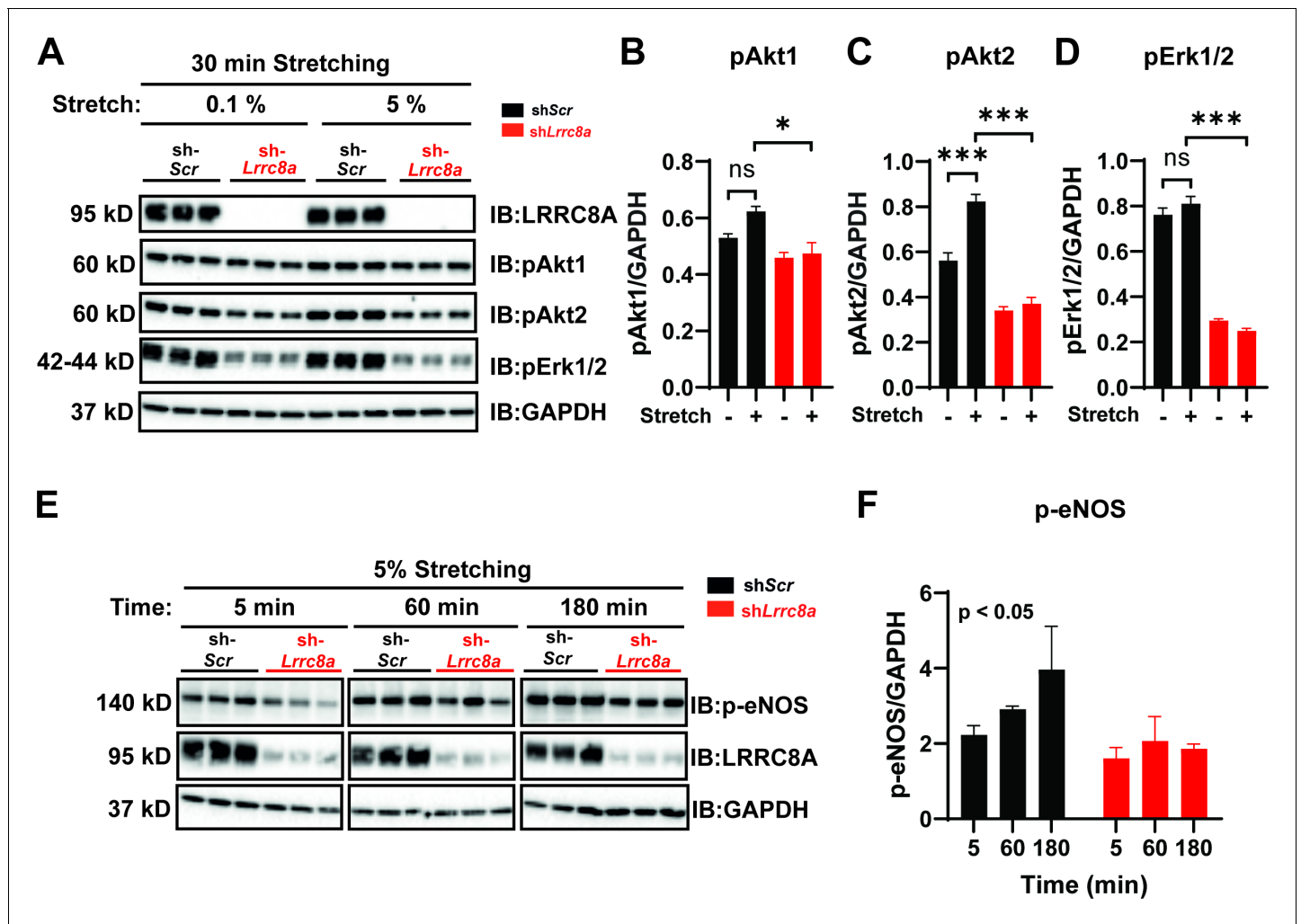


**Figure 4.** Leucine-rich repeat-containing protein 8a (LRRC8A) is required for intact stretch-induced AKT-endothelial nitric oxide synthase (eNOS) signaling. (A) Western blot of LRRC8A, pAKT1, pAKT2, pERK1/2 in response to 30 min of 0.1% and 5% static stretch in Ad-shScr (n = 3) and Ad-shLrrc8a (n = 3) transduced human umbilical vein endothelial cells (HUVECs). GAPDH is used as a loading control. (B–D) Densitometry quantification from A of pAKT1 (B), pAKT2 (C), and pErk1/2 (D). (E) Western blot of peNOS, LRRC8A, in response to 5% static stretching for 5, 60, and 180 min in Ad-shScr (n = 3) and Ad-shLrrc8a (n = 3) transduced HUVECs. (F) Densitometry quantification from E of eNOS. GAPDH is used as a loading control. Statistical significance between the indicated group is calculated using one-way analysis of variance (ANOVA), Tukey’s multiple comparisons test for (B–D), and two-way ANOVA for (F) with p-value in upper left corner. Data are shown as mean ± s.e.m. \*p<0.05; \*\*p<0.01; \*\*\*p<0.001. The online version of this article includes the following source data for figure 4:

**Source data 1.** Source data for **Figure 4F**.

**Source data 2.** Source data for **Figure 4B,C, D**.

particularly in the setting of HFHS diet. Also consistent with impaired eNOS activity are reductions in vessel number (**Figure 8E**), vessel surface area (**Figure 8H**), number of end points (**Figure 8K**), branching index (**Figure 8L**), and increased lacunarity (**Figure 8J**). These parameters are all suggestive of diabetes-induced retinal vessel dysfunction in the eLrrc8a KO mice, consistent with the loss of eNOS activity that is expected when insulin signaling is compromised (**Brooks et al., 2001; Kondo et al., 2003**). Notably, both WT and eLrrc8a KO mice were found to be equally glucose-intolerant and insulin-resistant (**Figure 8—figure supplement 3**), indicating that these differences in microvascular dysfunction were not due to increased hyperglycemia and more severe diabetes in eLrrc8a KO mice. However, while there were no differences in mean body weight or fat mass between WT and eLrrc8a KO males raised on HFHS diet (**Figure 8—figure supplement 4**), female eLrrc8a KO mice had higher body weights than WT female mice, and this was driven by an increase

in total fat mass (**Figure 8—figure supplement 4**). Taken together, our findings reveal that LRRC8A is highly expressed in endothelium and functionally encodes endothelial VRAC. LRRC8A regulates basal, stretch, and shear-flow-mediated ERK, AKT-eNOS signaling, forms an LRRC8A-GRB2-Cav1-eNOS signaling complex, and regulates vascular function in vivo.

## Discussion

Our findings demonstrate that the LRRC8 hetero-hexamer functionally encodes endothelial VRAC, whereby LRRC8A associates with GRB2 and Cav1 and positively regulates PI3K-AKT-eNOS and ERK1/2 signaling. LRRC8A depletion in HUVECs reduces pAKT2, pAKT1, p-eNOS, and pERK1/2 under basal conditions, and abrogates both stretch and shear-flow stimulated p-eNOS stimulation. We also discovered the ability of HUVECs to align along the direction of laminar shear flow is markedly impaired in LRRC8A KD cells – suggesting these cells have an impaired ability to either sense or respond to laminar shear flow (or both). These data reveal that LRRC8A-mediated PI3K-AKT signaling is conserved in endothelium, similar to previous observations in adipocytes (**Zhang et al., 2017**) and skeletal myotubes (**Kumar et al., 2020**), and in turn positively regulates eNOS expression and activity. Consistent with this mechanism, endothelial-targeted *Lrrc8a* ablation in vivo predisposes to microvascular dysfunction in the setting of T2D and to hypertension in response to Ang II infusion. These results are in line with the notion that LRRC8A depleted endothelium contributes to an insulin-resistant state in which impaired PI3K-AKT-eNOS signaling results in a propensity for vascular dysfunction (**Kearney et al., 2008; Muniyappa and Sowers, 2013**). Insulin-mediated regulation of NO is physiologically (**Zeng and Quon, 1996; Zeng et al., 2000; Montagnani et al., 2002**) and pathophysiologically (**Steinberg et al., 1996**) important, as NO has vasodilatory (**Quillon et al., 2015; Palmer et al., 1987**), anti-inflammatory (**Kataoka et al., 2002**), antioxidant (**Clapp et al., 2004**), and antiplatelet effects (**Schäfer et al., 2004a; Schäfer et al., 2004b; Radoski et al., 1987a; Radoski et al., 1987b**). Impaired NO-mediated vascular reactivity is a predictor of future adverse cardiac events (**Schächinger et al., 2000**) and portends increased risk of atherosclerosis (**Bugiardini et al., 2004**). Consistent with these NO-mediated effects, the RNA sequencing data derived from LRRC8A KD HUVECs revealed enrichment in inflammatory, cell adhesion, and proliferation pathways (GADD45, IL-8, mTOR, TREM1 signaling) that may arise from LRRC8A-mediated dysregulation of eNOS activity. Moreover, *Lrrc8a* mRNA is highly expressed in HUVECs relative to adipocyte and myotube cell lines examined previously (**Zhang et al., 2017; Kumar et al., 2020**), higher than many endothelial genes, and higher than other mechanosensitive (Piezo1) and mechanoresponsive (TRPV4) ion channels with well-established roles in endothelial biology (**Sonkusare et al., 2012; Rode et al., 2017; Li et al., 2014; Cappelli et al., 2019; Dalsgaard et al., 2016; Dunn et al., 2013; Earley et al., 2005; Harraz et al., 2018; Mercado et al., 2014; Sonkusare et al., 2014**).

In addition to reductions in AKT-eNOS signaling, LRRC8A depletion in HUVECs also reduced ERK1/2 signaling. This decrease in pERK1/2 suggests impaired MAPK signaling which is connected to the insulin receptor by GRB2-SOS. Indeed, we also found that LRRC8A and GRB2 interact in HUVECs, and this may provide the molecular mechanism for the observed defect in ERK signaling. Interestingly, GRB2-MAPK signaling is thought to promote angiogenesis, migration, and proliferation (**Zhao et al., 2011**), so reductions in ERK1/2 signaling would be predicted to inhibit these processes. One hypothesized mechanism of LRRC8A-mediated regulation of ERK1/2 and AKT2-eNOS signaling involves non-conductive protein-protein signaling via the LRRD as described previously in adipocytes (**Zhang et al., 2017; Gunasekar et al., 2019**). An alternative hypothesis is that LRRC8A-mediated VRAC channel activity may alter endothelial membrane potential to regulate other endothelial ion channels, such as Piezo1 or TRPV4, and downstream calcium signaling to influence downstream signaling. Future studies will further delineate the molecular mechanisms of LRRC8A regulation of intracellular signaling in endothelial cells and vascular function, and also directly explore whether endothelial LRRC8A-mediated VRAC channel complexes are themselves mechanoresponsive, as suggested in prior studies in other cell types (**Browe and Baumgarten, 2003; Browe and Baumgarten, 2006**).

Another curious observation that warrants further exploration is the reduction in basal *Akt2* and *NOS2* (eNOS) mRNA expression upon LRRC8A KD in HUVECs, which is also observed at the protein level. We can only speculate that LRRC8A is somehow regulating *Akt2* and *eNOS* gene expression.

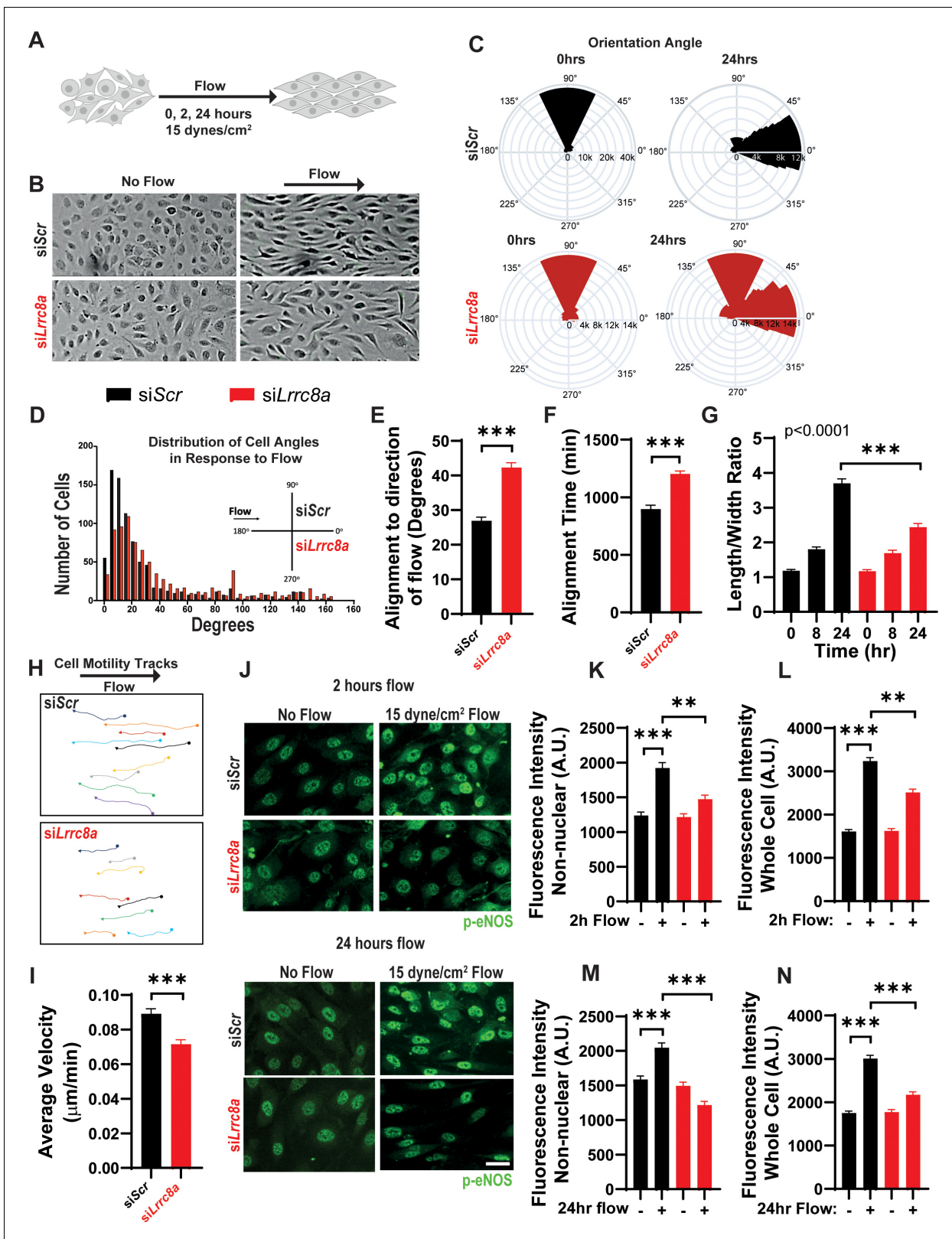


**Figure 5.** Leucine-rich repeat-containing protein 8a (LRRc8a) depletion impairs human umbilical vein endothelial cell (HUVEC) alignment to the direction of shear flow. (A) Cartoon of depicting the laminar shear flow applied to HUVEC at 15 dyne/cm<sup>2</sup> for 0, 2, and 24 hr. (B) Bright field image of HUVECs transfected with siScr (top) and siLrrc8a (bottom) with no flow (left) and after 24 hr of flow (right). (C) Distributions of angle of HUVEC orientation relative to the direction of flow at 0 hr and after 24 hr of laminar shear flow in siScr-treated cells (top, 0 hr: n = 800; 24 hr: n = 800) and siLrrc8a-treated cells (bottom, 0 hr: n = 800; 24 hr: n = 800). *Figure 5 continued on next page*

Figure 5 continued

siLrrc8a treated cells (bottom, 0 hr: n = 600; 24 hr: 800). Cuboidal or symmetrical cells at 0 hr were measured as 90° to the direction of flow. (D) Distributions of angle of HUVEC orientation relative to the direction of flow at 24 hr siScr (black, n = 803) and siLrrc8a treated cells (red, n = 803). (E) Mean alignment to direction of flow of siScr (black, n = 803) and siLrrc8a treated cells (red, n = 803). (F) Mean time required for HUVEC to align to within 20° of the direction of shear flow in siScr (black, n = 110) and siLrrc8a treated cells (red, n = 110). (G) Mean HUVEC length-width ratio over time upon stimulation with shear flow in siScr (black, n = 157) and siLrrc8a treated cells (red, n = 157). (H) Representative HUVEC real-time cell tracking during the 24 hr period of shear flow. Arrow heads represent the direction of travel against the direction of shear flow. (I) Average velocity calculated from the mean distance traveled over the 24 hr period of shear flow (n<sub>siScr</sub> = 77; n<sub>siLrrc8a</sub> = 78). (J) Representative phosphorylated endothelial nitric oxide synthase (p-eNOS) immunofluorescence (green) under conditions of no flow (n = 100), 2 hr (n = 100, top) and no flow (n = 110), 24 hr flow (n = 110, bottom). (K–L) Quantification of non-nuclear p-eNOS immunofluorescence (K) and whole-cell p-eNOS (L) under conditions of no flow (n = 100) and 2 hr flow (n = 100). (M–N) Quantification of non-nuclear p-eNOS immunofluorescence (M) and whole-cell p-eNOS (N) under conditions of no flow (n = 110) and 24 hr flow (n = 110). Statistical significance between the indicated values is calculated using a two-tailed Student's t-test for (E), (F), and (I), using one-way analysis of variance (ANOVA), Tukey's multiple comparisons test for (K), (L), (M), and (N), and using two-way ANOVA with Bonferroni multiple comparison test in (G). In (G), p < 0.001 for the time dependence of siScr versus siLrrc8a treated cells, and p < 0.001 for the 24 hr timepoint. Error bars represent mean ± s.e.m. n = 3, independent experiments. \*\*p < 0.01 and \*\*\*p < 0.001.

The online version of this article includes the following video, source data, and figure supplement(s) for figure 5:

**Source data 1.** Source data for **Figure 5E**.

**Source data 2.** Source data for **Figure 5F**.

**Source data 3.** Source data for **Figure 5G**.

**Source data 4.** Source data for **Figure 5I**.

**Source data 5.** Source data for **Figure 5K**.

**Source data 6.** Source data for **Figure 5L**.

**Source data 7.** Source data for **Figure 5M**.

**Source data 8.** Source data for **Figure 5N**.

**Figure supplement 1.** Leucine-rich repeat-containing protein 8a (LRRC8A) knock-down abrogates shear-flow stimulated phosphorylated endothelial nitric oxide synthase (p-eNOS) in human umbilical vein endothelial cells (HUVECs).

**Figure supplement 1—source data 1.** Source data for **Figure 5—figure supplement 1B**.

**Figure supplement 1—source data 2.** Source data for **Figure 5—figure supplement 1C**.

**Figure 5—video 1.** Bright field time-lapse video of siScr transfected human umbilical vein endothelial cell (HUVEC) responding to shear flow (direction of flow from left to right) over a 24 hr period.

<https://elifesciences.org/articles/61313#fig5video1>

**Figure 5—video 2.** Bright field time-lapse video of siScr transfected human umbilical vein endothelial cell (HUVEC) responding to shear flow (direction of flow from left to right) over a 24 hr period.

<https://elifesciences.org/articles/61313#fig5video2>

**Figure 5—video 3.** Bright field time-lapse video of siLrrc8a transfected human umbilical vein endothelial cell (HUVEC) responding to shear flow (direction of flow from left to right) over a 24 hr period.

<https://elifesciences.org/articles/61313#fig5video3>

**Figure 5—video 4.** Bright field time-lapse video of siLrrc8a transfected human umbilical vein endothelial cell (HUVEC) responding to shear flow (direction of flow from left to right) over a 24 hr period.

<https://elifesciences.org/articles/61313#fig5video4>

Both PI3K and ERK1/2 signaling pathways have been described to regulate total eNOS expression (Wu, 2002), and we observe reductions in both PI3K and ERK1/2 signaling in LRRC8A KD HUVECs, so reductions in eNOS expression are certainly consistent with disruptions in these signaling pathways. Consistent with this conserved biology with respect to LRRC8A signaling, we also observed significant twofold reductions in AKT2 expression upon *Lrrc8a* deletion in both 3T3-F442A adipocytes (Zhang et al., 2017) and C2C12 myotubes (Kumar et al., 2020), in addition to reductions in NOS2 (iNOS) (Kumar et al., 2020) in adipocytes and NOS1 (neuronal NOS) in C2C12 myotubes (Kumar et al., 2020). Collectively, these findings across multiple cell types support a PI3K and ERK1/2 mediated mechanism of regulation of eNOS and AKT2 gene expression.

The phenotype of endothelial-targeted *Lrrc8a* KO (*eLrrc8a* KO) mice are consistent with a reduction in eNOS and p-eNOS as these mice exhibit mild hypertension at baseline (females) and exacerbated hypertension in response to chronic angiotensin infusion, suggesting a modulatory effect on vascular reactivity. Similarly, retinal blood flow is only mildly impaired in *eLrrc8a* KO mice raised on a regular diet, with some evidence of microvascular disease. However, both retinal blood flow and retinal vessel morphology are markedly impaired in obese-T2D, insulin-resistant *eLrrc8a* KO mice raised on an HFHS diet compared to controls. This is consistent with a synergistic role of endothelial

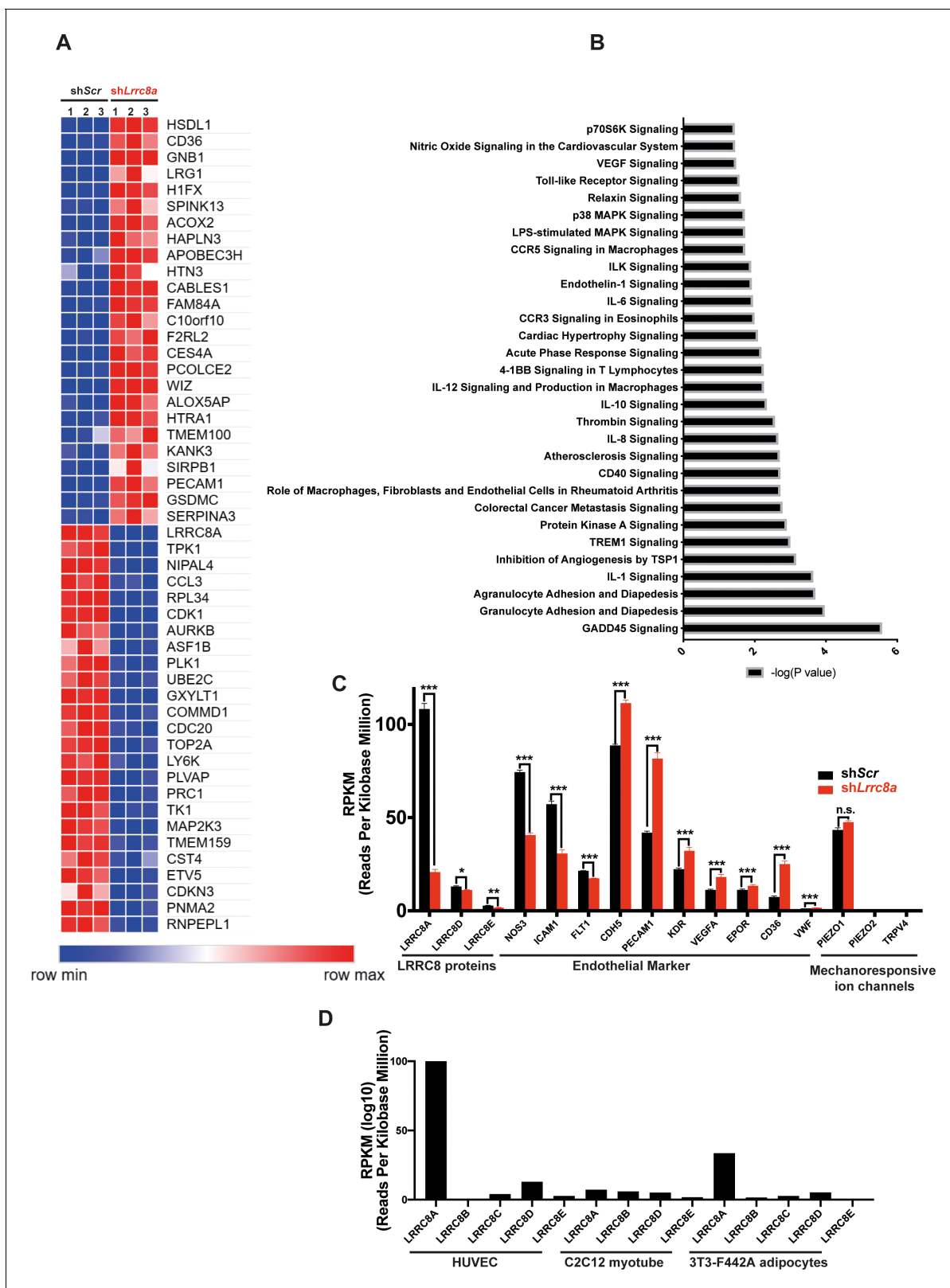


**Figure 6.** RNA sequencing of Ad-shScr and Ad-shLrrc8a transduced human umbilical vein endothelial cells (HUVECs). (A) Heatmap analysis displaying top 25 upregulated or 25 downregulated genes between shScr and shLrrc8a. (B) IPA canonical pathway analysis of genes significantly regulated by shLrrc8a in comparison to shScr n = 3 for each group. For analysis with Ingenuity Pathway Analysis (IPA), Fragments Per Kilobase of transcripts per Million mapped reads (FPKM) cutoffs of 1.5, fold change of 1.5, and false discovery rate <0.05 were utilized for significantly differentially regulated genes. (C) Bar chart showing RPKM values for Lrrc8 proteins, endothelial markers, and mechanoresponsive ion channels in HUVECs. (D) Bar chart showing RPKM values for Lrrc8 genes in HUVEC, C2C12 myotube, and 3T3-F442A adipocytes. Figure 6 continued on next page

Figure 6 continued

genes. (C) Expression levels of select *LRRC8* mRNA, classic endothelial markers, and mechanoresponsive ion channels in shScr and sh*Lrrc8a*-treated HUVECs. (D) Expression levels *LRRC8a-e* mRNA in HUVECs compared to data previously published from C2C12 myotubes (Kumar et al., 2020) and differentiated 3T3-F442A adipocytes (Zhang et al., 2017). For (C), statistical significance between the indicated values was calculated using an unpaired two-tailed Student's t-test. Error bars represent mean ± s.e.m. n = 3, independent experiments. \*p<0.05; \*\*p<0.01; \*\*\*p<0.001.

The online version of this article includes the following source data for figure 6:

**Source data 1.** Source data for **Figure 6C**.

**Source data 2.** Source data for **Figure 6D**.

*eLrrc8a* ablation and T2D/obesity in the pathogenesis of vascular disease. Our results suggest that reductions in LRRC8A signaling may contribute to impaired vascular function observed in humans in response to insulin and/or shear stress in the setting of obesity (Arcaro et al., 1999; Tack et al., 1998; Westerbacka et al., 1999; Williams et al., 2006) and insulin resistance (Murphy et al., 2007).

## Materials and methods

### Key resources table

Reagent type (species) or resource	Designation	Source or reference	Identifiers	Additional information
Genetic reagent ( <i>Mus musculus</i> )	<i>eLrrc8a</i> KO ( <i>Lrrc8a<sup>fl/fl</sup></i> )	This paper	Sah lab	SWELL1 is a regulator of adipocyte size, insulin signaling, and glucose homeostasis (Zhang et al., 2017)
Strain, strain background ( <i>Mus musculus</i> )	<i>CDH5-Cre</i>	Gift from Dr. Kaikobad Irani		Vikram, A, <i>Nature Communications</i> 2016
Strain, strain background ( <i>Mus musculus</i> )	<i>Rosa26-tdTomato</i>	Jackson lab	Jax 007914 RRID:IMSR_JAX:007914	
Other	HUVECs	ATCC	Cat#CRL-2922 RRID:CVCL_3901	Human primary cells
Biological sample ( <i>Mus musculus</i> )	Endothelial primary cell	<i>Lrrc8a<sup>fl/fl</sup></i>		Freshly isolated from <i>Lrrc8a<sup>fl/fl</sup></i> mice
Antibody	Anti-β-actin (rabbit monoclonal)	Cell Signaling	Cat#8457s, RRID:AB_10950489	WB (1:2000)
Antibody	Anti-total Akt (rabbit monoclonal)	Cell Signaling	Cat#4685s, RRID:AB_2225340	WB (1:1000)
Antibody	Anti-Akt1 (rabbit monoclonal)	Cell Signaling	Cat#2938s, RRID:AB_915788	WB (1:1000)
Antibody	Anti-p-eNOS (rabbit monoclonal)	Cell Signaling	Cat#9571, RRID:AB_329837	WB (1:1000) IF (1:200)
Antibody	Anti-p-eNOS (rabbit polyclonal)	Invitrogen	Cat#PA5-104858, RRID:AB_2816331	IF (1:200)
Antibody	Anti-Akt2 (rabbit monoclonal)	Cell Signaling	Cat#3063s, RRID:AB_2225186	WB (1:1000)
Antibody	Anti-p-AS160 (rabbit polyclonal)	Cell Signaling	Cat#4288s, RRID:AB_10545274	WB (1:1000)
Antibody	Anti-total eNOS (rabbit polyclonal)	Cell Signaling	Cat#32027, RRID:AB_2728756	WB (1:1000)
Antibody	Anti-PECAM (rabbit monoclonal)	Sigma	Cat#SAB4502167 RRID:AB_10762600	WB (1:1000)
Antibody	Anti-VEGFR2 (goat polyclonal)	R and D Systems	Cat#BAF357 RRID:AB_356414	WB (1:1000)

Continued on next page

Continued

Reagent type (species) or resource	Designation	Source or reference	Identifiers	Additional information
Antibody	Anti- pS6 ribosomal (rabbit monoclonal)	Cell Signaling	Cat#5364s, RRID:AB_10694233	WB (1:2000)
Antibody	Anti- GAPDH (rabbit monoclonal)	Cell Signaling	Cat#5174s, RRID:AB_1062202	WB (1:2000)
Antibody	Anti-pErk1/2 (rabbit polyclonal)	Cell Signaling	Cat#9101s, RRID:AB_331772	WB (1:1000)
Antibody	Anti-Total Erk1/2 (rabbit polyclonal)	Cell Signaling	Cat#9102s, RRID:AB_330744	WB (1:1000)
Antibody	Anti-Grb2 (mouse monoclonal)	BD	Cat#610111s, RRID:AB_397517	WB (1:1000)
Antibody	Anti-Grb2 (rabbit monoclonal)	Santa Cruz	Cat#sc-255, RRID:AB_631602	WB (1:1000)
Antibody	Anti-LRRC8A (rabbit polyclonal)	Pacific antibodies	Custom made	Epitope: QRTKSRIEQGIVDRSE, WB (1:1000), LRRC8A is a glucose sensor regulating $\beta$ -cell excitability and systemic glycemia ( <i>Kang et al., 2018</i> )
Antibody	Anti-CD31 (rabbit polyclonal)	Thermo Fisher	Cat#MA3105, RRID:AB_223592	IF (1:100)
Antibody	Anti-IgG (normal mouse IgG)	Santa Cruz	Cat#sc-2027, RRID:AB_737197	WB (1:1000)
Antibody	Anti-rabbit-HRP	BioRad	Cat#170-6515, RRID:AB_11125142	WB (1:10,000)
Antibody	Anti-mouse-HRP	BioRad	Cat#170-5047, RRID:AB_11125753	WB (1:10,000)
Transfected construct (human)	siLrrc8a	Invitrogen	Cat#4392420	Assay ID: s32107 Transfected construct human
Transfected construct (human)	Non-targeting control	Invitrogen	Cat#4390846	Transfected construct human
Transfected construct (human)	siPORTamine	Invitrogen	Cat#AM4503	
Transfected construct (human)	Opti-MEM	Invitrogen	Cat#11058-021	
Recombinant DNA reagent	Ad5-U6-hLrrc8a-shRNA-mCherry	Vector biolabs	shADV-653 214592	
Recombinant DNA reagent	Ad5-U6-Scr-shRNA-mCherry	Vector biolabs	3086	
Commercial assay or kit	RNA isolation (PureLink RNA mini kit)	Invitrogen	12183018A	
Software, algorithm	GraphPad Prism8		La Jolla California USA, <a href="http://www.graphpad.com">http://www.graphpad.com</a> RRID:SCR_002798	
Software, algorithm	Fiji, ImageJ	<i>Schindelin et al., 2012</i> (PMID:22743772)	RRID:SCR_002285	
Other	DAPI stain	Thermofisher	Cat#T3605	1:10,000

## Animals

The institutional animal care and use committee of the University of Iowa and Washington University School of Medicine approved all experimental procedures involving animals. All mice were housed in temperature, humidity, and light controlled environment and allowed water access and food. Both male and female *Lrrc8a<sup>fl/fl</sup>* (*Zhang et al., 2017; Kang et al., 2018*) (WT), *CDH5-Cre;Lrrc8a<sup>fl/fl</sup>* (*eLrrc8a*

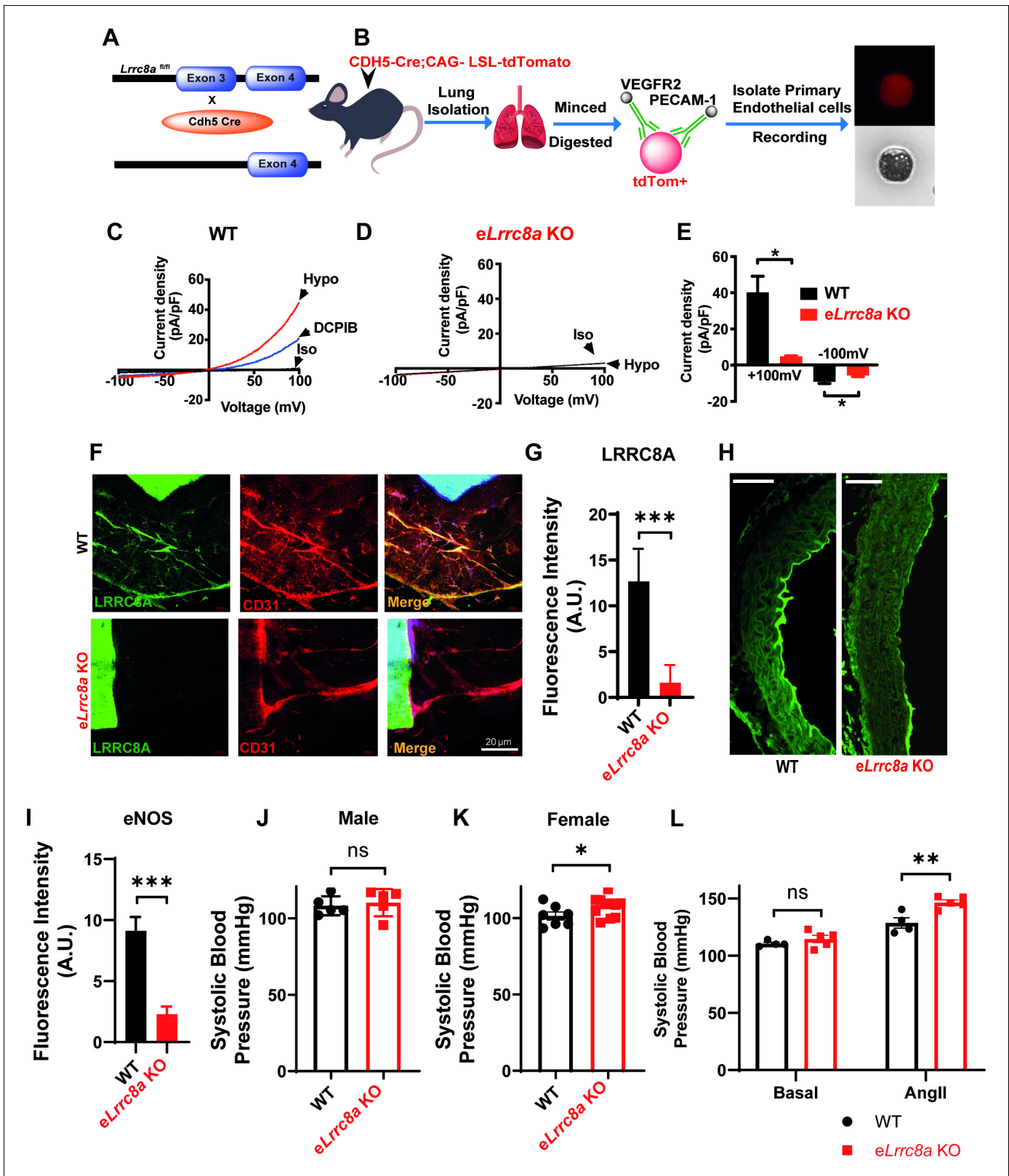


**Figure 7.** Endothelial-targeted *Lrrc8a* KO mice exhibit reduced phosphorylated endothelial nitric oxide synthase (p-eNOS) and mild angiotensin-II stimulated hypertension. (A) Strategy for endothelium targeted *Lrrc8a* ablation to generate *eLrrc8a* KO. (B) Isolation of murine primary endothelial cells from WT and *eLrrc8a* KO using tdTomato reporter mice. (C–D) Current-voltage relationships of volume-regulatory anion channel (VRAC) current in isotonic (Iso, 300 mOsm) and hypotonic (Hypo, 210 mOsm) solution in response to voltage ramps from -100 to +100 mV over 500 ms in WT (C) and KO (D). (E) Current density (pA/pF) in response to voltage ramps from -100 to +100 mV over 500 ms in WT (black) and *eLrrc8a* KO (red). (F) Fluorescence images of WT (top) and *eLrrc8a* KO (bottom) for LRRC8A (green) and CD31 (red). (G) Bar graph of LRRC8A fluorescence intensity (A.U.) in WT (black) and *eLrrc8a* KO (red). (H) Fluorescence images of WT (left) and *eLrrc8a* KO (right). (I) Bar graph of eNOS fluorescence intensity (A.U.) in WT (black) and *eLrrc8a* KO (red). (J) Systolic Blood Pressure (mmHg) in Male WT (black) and *eLrrc8a* KO (red) (ns). (K) Systolic Blood Pressure (mmHg) in Female WT (black) and *eLrrc8a* KO (red) (\*). (L) Systolic Blood Pressure (mmHg) in Basal (left) and AngII (right) conditions for WT (black) and *eLrrc8a* KO (red) (ns for Basal, \*\* for AngII).

Figure 7 continued

(D) primary murine endothelial cells. DCPIB (10  $\mu$ M) inhibition in C (WT). (E) Mean outward (+100 mV) and inward (-100 mV) currents from WT (n = 3 cells) and *eLrrc8a* KO (n = 3 cells). (F) Ex vivo aorta sprouting assay performed in aortic rings isolated from WT and *eLrrc8a* KO mice and cultured in FGM media for 3 days at 37°C. Immunofluorescence staining with antibodies to LRRC8A (green), CD31 (red), LRRC8A+CD31+ (Merge) demonstrating endothelial-targeted *Lrrc8a* deletion. (G) Quantification of LRRC8A immunofluorescence staining in WT (n = 15) and *eLrrc8a* KO (n = 15) endothelial cell tubes. (H–I) Representative images of aortic sections from WT (n = 3) and *eLrrc8a* KO (n = 3) mice immunostained with p-eNOS (H, green), and immunofluorescence quantification of regions of WT (n = 5) and *eLrrc8a* KO (n = 5) endothelium (I). Scale bar in (H) is 50  $\mu$ m. (J–L) Tail-cuff systolic blood pressures of male (J) and female (K) WT (n = 5 males and 7 females) and *eLrrc8a* KO (n = 5 males and 12 females) mice, and systolic blood pressures of male WT (n = 4) and *eLrrc8a* KO (n = 5) mice under basal conditions and after 4 weeks of chronic angiotensin-II infusion (L). Statistical significance between the indicated values is calculated using a two-tailed unpaired Student's t-test. Error bars represent mean  $\pm$  s.e.m. \*p<0.05; \*\*p<0.01; \*\*\*p<0.001.

The online version of this article includes the following source data for figure 7:

**Source data 1.** Source data for **Figure 7E**.

**Source data 2.** Source data for **Figure 7I**.

**Source data 3.** Source data for **Figure 7J**.

**Source data 4.** Source data for **Figure 7K**.

**Source data 5.** Source data for **Figure 7L**.

KO) mice were generated and used in these studies. *CDH5-Cre* mice were obtained from Dr. Kaikobad Irani (University of Iowa, IA). In a subset of experiments, 5–8 week old *Lrrc8a<sup>fl/fl</sup>* and *CDH5-Cre; Lrrc8a<sup>fl/fl</sup>* mice were switched to HFHS (high-fat high-sucrose rodent diet, Research Diets, Inc, Cat# D12331) for at least 10 months. *CDH5-Cre* mice were crossed with *Rosa26-tdTomato* (Jax# 007914) reporter mice to identify CDH5+ cells for primary endothelium patch-clamp studies.

## Antibodies

Rabbit polyclonal anti-LRRC8A antibody was generated against the epitope QRTKSRIEQGIVDRSE (Pacific Antibodies) (Kang et al., 2018). All other primary antibodies were purchased from Cells Signaling: anti- $\beta$ -actin (#8457), Total Akt (#4685S), Akt1 (#2938), Akt2 (#3063), p-eNOS (#9571), Total eNOS (#32027), p-AS160 (#4288), p-p70 S6 Kinase (#9205S), pS6 Ribosomal (#5364S), GAPDH (#5174), pErk1/2 (#9101), Total Erk1/2 (#9102). Anti-LRRC8A antibody was custom made as described previously (Zhang et al., 2017; Kang et al., 2018). A second p-eNOS antibody was purchased from Invitrogen (Cat#PA5-104858) and used to compare with anti-p-eNOS from Cell Signaling (#9571) for p-eNOS IF staining. Purified mouse anti-Grb2 was purchased from BD (610111) and Santa Cruz (#sc-255). Rabbit IgG was purchased from Santa Cruz (sc-2027). Anti-CD31 was purchased from Thermo Fisher (MA3105).

## Electrophysiology

All recordings were performed in the whole-cell configuration at room temperature (RT), as previously described (Zhang et al., 2017; Kang et al., 2018). Briefly, currents were measured with either an Axopatch 200B amplifier or a MultiClamp 700B amplifier (Molecular Devices) paired to a Digidata 1550 digitizer. Both amplifiers used pClamp 10.4 software. The intracellular solution contained (in mM): 120 L-aspartic acid, 20 CsCl, 1 MgCl<sub>2</sub>, 5 EGTA, 10 HEPES, 5 MgATP, 120 CsOH, 0.1 GTP, pH 7.2 with CsOH. The extracellular solution for hypotonic stimulation contained (in mM): 90 NaCl, 2 CsCl, 1 MgCl<sub>2</sub>, 1 CaCl<sub>2</sub>, 10 HEPES, 5 glucose, 5 mannitol, pH 7.4 with NaOH (210 mOsm/kg). The isotonic extracellular solution contained the same composition as above except for mannitol concentration of 105 (300 mOsm/kg). The osmolarity was checked by a vapor pressure osmometer 5500 (Wescor). Currents were filtered at 10 kHz and sampled at 100  $\mu$ s interval. The patch pipettes were pulled from borosilicate glass capillary tubes (WPI) by a P-87 micropipette puller (Sutter Instruments). The pipette resistance was ~4–6 MO when the patch pipette was filled with intracellular solution. The holding potential was 0 mV. Voltage steps (500 ms) were elicited from 0 mV holding potential from -100 to +100 mV in 20 mV increments every 0.6 s. Voltage ramps from -100 to +100 mV (at 0.4 mV/ms) were applied every 4 s.

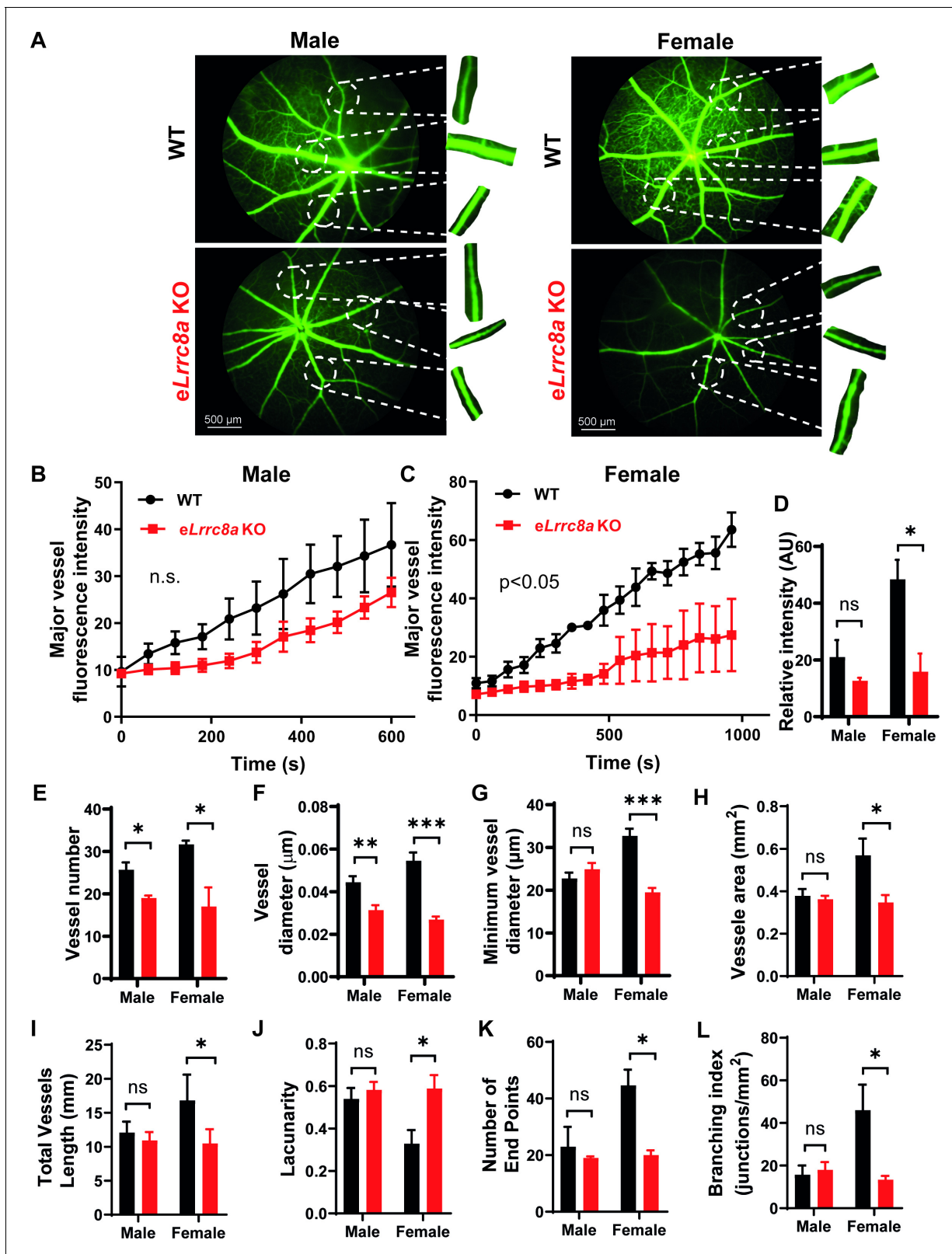


**Figure 8.** Endothelium-specific *Lrrc8a* KO mice exhibit exacerbated impairments retinal microvascular disease in the setting of type 2 diabetes. (A) Representative fluorescein retinal angiograms of WT (top) and *eLrrc8a* KO (bottom) male (left) and female (right) mice raised on a high-fat high-sucrose (HFHS) diet. Inset shows magnified view of retinal vessels. Quantification of major vessel fluorescence intensity over time after intraperitoneal (i.p.) fluorescein injection in (B) male (n = 3) and (C) female (n = 3) WT and *eLrrc8a* KO mice. (D–K) Quantification of total retinal vessel intensity (D), total vessel length (E), vessel diameter (F), minimum vessel diameter (G), vessel area (H), total vessel length (I), lacunarity (J), number of end points (K), and branching index (L). \*p < 0.05, \*\*p < 0.01, \*\*\*p < 0.001, ns = not significant. Figure 8 continued on next page

Figure 8 continued

vessel number (E), vessel diameter (F), minimum vessel diameter (G), vessel area (H), total vessel length (I), lacunarity (J), number of end points (K), and branching index (L) of retinal vessels in WT and *eLrrc8a* KO mice. Statistical significance between the indicated values for B and C was calculated using two-way analysis of variance (ANOVA) and (D–L) using a two-tailed unpaired Student's t-test. Error bars represent mean  $\pm$  s.e.m. \* $p < 0.05$ ; \*\* $p < 0.01$ ; \*\*\* $p < 0.001$ .

The online version of this article includes the following video, source data, and figure supplement(s) for figure 8:

**Source data 1.** Source data for **Figure 8B**.

**Source data 2.** Source data for **Figure 8C**.

**Source data 3.** Source data for **Figure 8D**.

**Source data 4.** Source data for **Figure 8E**.

**Source data 5.** Source data for **Figure 8F**.

**Source data 6.** Source data for **Figure 8G**.

**Source data 7.** Source data for **Figure 8H**.

**Source data 8.** Source data for **Figure 8I**.

**Source data 9.** Source data for **Figure 8J**.

**Source data 10.** Source data for **Figure 8K**.

**Source data 11.** Source data for **Figure 8L**.

**Figure supplement 1.** Endothelium-specific *Lrrc8a* KO mice exhibit mild retinal microvascular disease at baseline.

**Figure supplement 1—source data 1.** Source data for **Figure 8—figure supplement 1C**.

**Figure supplement 1—source data 2.** Source data for **Figure 8—figure supplement 1D**.

**Figure supplement 1—source data 3.** Source data for **Figure 8—figure supplement 1E**.

**Figure supplement 1—source data 4.** Source data for **Figure 8—figure supplement 1F**.

**Figure supplement 1—source data 5.** Source data for **Figure 8—figure supplement 1G**.

**Figure supplement 1—source data 6.** Source data for **Figure 8—figure supplement 1H**.

**Figure supplement 1—source data 7.** Source data for **Figure 8—figure supplement 1I**.

**Figure supplement 1—source data 8.** Source data for **Figure 8—figure supplement 1J**.

**Figure supplement 1—source data 9.** Source data for **Figure 8—figure supplement 1K**.

**Figure supplement 2.** Endothelium-specific *Lrrc8a* KO mice exhibit exacerbated impairments retinal microvascular disease in the setting of type 2 diabetes.

**Figure supplement 3.** Glucose tolerance (GTT) and insulin tolerance (ITT) are not altered in endothelium-specific *Lrrc8a* KO mice ( $n = 13$ ) compared to WT mice ( $n = 8$ ) raised on a high-fat high-sucrose diet for 10 months.

**Figure supplement 3—source data 1.** Source data for **Figure 8—figure supplement 3**.

**Figure supplement 4.** Body weight and body composition of WT and endothelium-specific *Lrrc8a* KO mice raised on a high-fat high-sucrose diet for 10 months.

**Figure supplement 4—source data 1.** Source data for **Figure 8—figure supplement 4**.

**Figure 8—video 1.** Retinal angiograms of WT (left) and *eLrrc8a* KO (right) upon fluorescein injection intraperitoneally.

<https://elifesciences.org/articles/61313#fig8video1>

## Adenoviral KD

HUVECs were plated at 550,000 cell/well in 12-well plates. Cells were grown for 24 hr in the plates and transduced with either human adenovirus type 5 with sh*Lrrc8a* (sh*Lrrc8a*: Ad5-mCherry-U6-h*Lrrc8a*-shRNA,  $2.2 \times 10^{10}$  PFU/ml [shADV-214592], Vector Biolabs) or a scrambled non-targeting control (shScr: Ad5-U6-scramble-mCherry,  $1 \times 10^{10}$  PFU/ml) at a multiplicity of infection of 50 for 12 hr, and studies performed 3–4 days after adenoviral transduction. The shLRRC8a targeting sequence is: GCA CAA CAT CAA GTT CGA CGT.

## siRNA KD

HUVECs were plated at 360,000 cell/well in six-well plates. Cells were grown for 24 hr (90–95% confluency) and transduced with either a silencer select siRNA with siLRRC8a (Cat#4392420, sense: GCAACUUCUGGUUCAAUUUTT antisense: AAUUUGAACCAGAAGUUGCTG, Invitrogen) or a non-targeting control silencer select siRNA (Cat#4390846, Invitrogen), as described previously (Koh et al., 2008). The siLRRC8a used targets a different sequence from the shRNA described above. Briefly, siRNAs were transduced twice, 24 and 72 hr after HUVEC plating. Each siRNA was combined with Opti-MEM (285.25  $\mu$ l, Cat#11058-021, Invitrogen) siPORT amine (8.75  $\mu$ l, Cat#AM4503, Invitrogen) and the silencer select siRNA (6  $\mu$ l) in a final volume of 300  $\mu$ l. HUVECs were transduced over a 4 hr period at 37°C, using DMEM +1% FBS. After transduction, the cells

were returned to media containing M199, 20% FBS, 0.05 g heparin sodium salt, and 15 mg ECGS. Cell lysates were collected at basal conditions on day 4.

### Isolation of mouse lung endothelial cells

Isolation of mouse lung endothelial cells was performed according to the following protocol: Day 1 – Incubate sheep anti-rat IgG Dynabeads (Invitrogen) overnight with PECAM (Sigma, #SAB4502167) and VEGFR2 (R and D Systems, #BAF357) antibodies at 4°C in PBS with gentle agitation. Day 2 – Lungs were removed from the mice, washed in 10% FBS/DMEM, minced into 1–2 mm squares, and digested with Collagenase Type I (2 mg/ml, Gibco) at 37°C for 1 hr with agitation. The cellular digest was filtered through a 70 µm cell strainer, centrifuged at 1500 rpm, and the cells immediately incubated with the antibody coated Dynabeads at RT for 20 min. The bead-bound cells were recovered with a magnet, washed two times with PBS, and plated overnight on collagen type I (100 µg/ml) coated coverslips. The endothelial cells were maintained in a growth media of M199, 20% FBS, 0.05 g heparin sodium salt, 50 mg/ml ECGS, and 1× anti-anti.

### Cell culture

HUVECs were purchased from ATCC and were grown in MCDB-131-complete media overnight. HUVECs for basal condition collection were grown in growth media of M199, 20% FBS, 0.05 g heparin sodium salt (Cat#9041-08-1, Alfa Aesar), and 15 mg ECGS (Cat#02-102, Millipore Sigma). Cells were routinely cultured on 1% of gelatin-coated plates at 37°C at 5% CO<sub>2</sub>. For insulin stimulation (Cat#SLBW8931), cells were serum starved for at least 13 hr in 1% FBS (Atlanta Bio selected, Cat#S11110) or without FBS using endothelial cells growth basal medium (Lonza Cat#cc-3121) instead of MCDB-131-complete media. Insulin stimulation was used for the times indicated at 100 nM.

### Immunoblotting

Cells were harvested in ice-cold lysis buffer (150 mM NaCl, 20 mM HEPES, 1% NP-40, 5 mM EDTA, pH 7.5) with added proteinase/phosphatase inhibitor (Roche). Cells were kept on ice with gentle agitation for 20 min to allow complete lysis. Lysate scraped into 1.5 ml tubes and cleared of debris by centrifugation at 14,000 × g for 20 min at 4°C. Supernatants were transferred to fresh tube and solubilized protein was measured using a DC protein assay kit (Bio-Rad). For immunoblotting, an appropriate volume of 1× Laemmli (Bio-Rad) sample loading buffer was added to the sample (10 µg of protein), which then heated at 90°C for 5 min before loading onto 4–20% gel (Bio-Rad). Proteins were separated using running buffer (Bio-Rad) for 2 hr at 150 V. Proteins were transferred to PVDF membrane (Bio-Rad) and membrane blocked in 5% (w/v) BSA in TBST or 5% (w/v) milk in TBST at RT for 2 hr. Blots were incubated with primary antibodies at 4°C overnight, followed by secondary antibody (Bio-Rad, Goat-anti-mouse #170–5047, Goat-anti-rabbit #170–6515, all used at 1:10,000) at RT for 1 hr. Membranes were washed three times and incubated in enhanced substrate Clarity (Bio-Rad) and imaged using a ChemiDoc XRS using Image Lab (Bio-Rad) for imaging and analyzing protein band intensities. β-Actin or GAPDH levels were quantified to correct for protein loading.

### Immunoprecipitation

Cells were seeded on gelatin-coated 10 cm dishes in complete media for 24 hr. Adenoviruses, Ad5-mCherry-U6-hLrrc8a-shRNA or Ad5-U6-Scr-mCherry were added to cells for 12 hr. After 4 days cells were serum starved for 16 hr with basal media containing 1% serum before stimulation with insulin (10 nM/ml). Cells were harvested in ice-cold lysis buffer (150 mM NaCl, 20 mM HEPES, 1% NP-40, 5 mM EDTA, pH 7.5) with added proteinase/phosphatase inhibitor (Roche) and kept on ice with gentle agitation for 15 min to allow complete lysis. Lysates were incubated with anti-Grb2 antibody (20 µg/ml) or control rabbit IgG (20 µg/ml, Santa Cruz sc-2027) rotating end over end overnight at 4°C. Protein G Sepharose beads (GE) were added to this for a further 4 hr before samples were centrifuged at 10,000 × g for 3 min and washed three times with RIPA buffer and re-suspended in laemmli buffer (Bio-Rad), boiled for 5 min, separated by SDS-PAGE gel followed by the Western blot protocol.

## Stretch assay

Equal amounts of cells were plated in each well in six well plated BioFlex coated with Laminin (BF-3001CCase) culture plate and seeded to ~90% confluence. Plates were placed into a FlexCell Jr. Tension System (FX-6000T) and incubated at 37°C with 5% CO<sub>2</sub>. Prior to stretch stimulation, basal media of 1% FBS was added for 16 hr. Cells on flexible membrane were subjected to static stretch with the following parameter: a stretch of 0.1% and 5% with static strain. Cells were stretched for 5, 30, 60, or 180 min. Cells were then lysed and protein isolated for subsequent Western blots.

## Laminar flow studies

HUVECs were grown in 1× M199 media (Gibco, Cat#11043-023) supplemented with 20% FBS (Gibco, Cat#16140-071), 50 mg bovine hypothalamus extract, and 0.01% heparin until full confluence in six-well plates. The cells were transfected twice across 3 days with 100 nM of siRNA for the *Lrrc8a* gene (si*Lrrc8a*) (Invitrogen, Cat#4392421, assay #:s32107) and a negative siRNA control (siControl) (Invitrogen, Cat#43900846) using siPORTAmine transfection agent (Invitrogen, Cat#AM4503) following the manufacturer recommendations (Koh *et al.*, 2008). Twenty-four hours after the final siRNA treatment, cells were transferred to  $\mu$ -Slide 0.4 I Luer slide (iBidi, Cat#80176) and incubated overnight at 37°C, 5% CO<sub>2</sub>, and 95% humidity. The slides were then cultured for 24 hr in a microscope stage incubator (Invitrogen, EVOS7000) under conditions of constant laminar flow at 15 dynes/cm<sup>2</sup>/s (Flocel Inc, Cat#QPL1010) and images acquired every 20 min. The peristaltic pump was converted to be laminar through the utilization of dampers on the outflow tracts of the pump. Efficacy in the generation of laminar flow was confirmed through the imaging of Q-Dots in the circulating media prior to the experiment (Invitrogen, Cat#Q21721MP). At the termination of the experiment, the cells were rinsed with 1× PBS and fixed with 4% paraformaldehyde (PFA) for downstream immunostaining applications.

## Immunostaining for laminar flow studies

To detect the levels of p-eNOS, the cell monolayer was stained with the anti-rabbit polyclonal antibody p-eNOS (Invitrogen, Cat#PA5104858 or Cell Signaling, Cat#9571), at a final dilution of 1:200 and a secondary anti-rabbit GFP AlexaFluor 488 (Invitrogen, Cat#R37116) at 1:2000 dilution. The slides were immunostained following the basic protocol: (1) 30 min RT incubation in Tris-Glycine; (2) 1 hr RT incubation  $\pm$  permeabilization with 0.01% TritonX-100; (3) 2 hr RT incubation in blocking solution (5% Sheep Serum, 1% Roche Blocking Buffer in PBST); (4) 1 hr at RT – overnight 4°C incubation with 1:200 primary antibody unless otherwise noted; (5) wash with PBST; (6) 2–3 hr RT incubation with 1:2000 secondary antibody in 5% Sheep Serum, 1% Roche Blocking Buffer in PBST; (7) wash with PBST and imaging analysis. The samples were observed under light microscopy using a Nikon Ti2. Quantification of immunostaining intensity was performed using ImageJ/Fiji (Schindelin *et al.*, 2012).

## Immunofluorescence imaging

Cells were plated on gelatin-coated glass coverslips. Cells on coverslip were washed in PBS and fixed with 2% (w/v) PFA for 20 min at RT. PFA was washed three times with PBS and permeabilized in PBS containing 0.2% Triton X-100 for 5 min at RT. Cells on coverslips were washed in PBS and blocked for 30 min at RT with TBS containing 0.1% Tween-20% and 5% BSA. Cells on coverslip were incubated overnight at 4°C with primary antibody (1:250) in TBS containing 0.1% Tween-20% and 1% BSA. Cells were then washed in PBS five times and incubated for 2 hr at RT with 5% BSA in TBST. Cells were washed three times in TBST and then incubated with secondary antibodies at 1:1000 dilution (Invitrogen, Anti-Rabbit 488, A11070; Anti-mouse 568, A11019; Anti-mouse 488, A11017) for 1 hr at RT. Coverslips were then incubated for 10 min with Topro 3 (T3605, Thermofisher) or mounted with mounting media containing DAPI (Invitrogen) to visualize nuclei. Images were taken using Axio-cam 503 Mono Camera controlled by Zeiss Blue using a Plan-Apochromate 40× oil immersion objective.

## Immunohistochemistry of thoracic aorta sections

Mouse thoracic aortas were dissected and immediately fixed in 10% formalin. The formalin fixed aortas were embedded in paraffin and 5  $\mu$ m sections were cut by automated microtome and mounted

on positively charged slides. Slides were deparaffinized with Histoclear and hydrated with 100% ethanol, 75% ethanol, 50% ethanol, and then distilled water. To achieve the antigen retrieval, slides were steamed in Citrate buffer at pH 6 (DAKO Target retrieval buffer S1699, DAKO) for 30 min and subsequently cooled for 30 min. Furthermore, to inhibit the endogenous peroxides, slides were quenched with 3% H<sub>2</sub>O<sub>2</sub> for 10 min. Slides were washed with distilled water, then 1× PBS and blocked with 1% BSA in 1× PBS for 1 hr. After washing with 1× PBS, slides were incubated with p-eNOS antibody (1:500 dilution) overnight in the humidified chamber at 4°C. Slides were washed two times with 1× PBS and incubated with secondary antibody (AF488, Invitrogen, 1:1000 dilution) for 1 hr. Subsequently slides were washed with 1× PBS three times and mounted with DAPI added mounting media with coverslip. The slides were imaged by Zeiss LSM700 confocal microscope (10× objective).

### Ex vivo sprouting angiogenesis

Following Avertin injection and cervical dislocation, aortas were dissected and connective tissue removed, and then washed with PBS with 50 µg/ml penicillin and streptomycin. Using iris scissors, the aorta was cut into aortic rings of 1–2 mm cross-sectional slices; 50 µl of Matrigel was used to coat the center of coverslips in 24-well plates for 2 hr at 37°C in the incubator to solidify the Matrigel. Aorta rings were then seeded and transplanted on Matrigel (BD Biosciences, Cat#356231) on coverslips. After seeding the aortic rings, plates were incubated at 37°C without medium for 10 min to allow the ring to attach to the Matrigel. Complete medium was added to each well and incubated at 37°C with 5% CO<sub>2</sub> for 48–72 hr. Phase contrast photos of individual explants were taken using a 10×/0.75 NA objective Olympus IX73 microscope (Olympus, Japan) fitted with camera (Orca flash 4.0+, Hamamatsu, Japan). Cells were incubated with LRRC8A (1:250) and CD31 (1:250) primary antibodies in 0.1% Tween-20% and 1% BSA overnight, and then incubated with secondary antibodies (Invitrogen, Anti-Rabbit 488, A11070; Anti-Mouse 568, A11019). Cells were then incubated for 10 min with Topro 3 (T3605, ThermoFisher) at RT.

### Retinal imaging

Ketamine (Akorn Animal Health, 100 mg/ml) was prepared and mixed with xylazine, then stored at RT. Animals were anesthetized with 87.5/12 mg/kg body weight via i.p. injection. Eyes were topically anesthetized with proparacaine and dilated with tropicamide. Fluorescein (100 mg/ml, Akorn Inc) diluted with sterile saline was administered by i.p. injection (50 µl), and mice were positioned on Micron imaging platform. Images of the eyes were taken from the start of fluorescein infusion with the Micron camera with a 450–650 nm excitation filter and 469–488 nm barrier filter at 30 frame/s using Micron software for 30 s. Data were converted into tiff image for further analysis.

### Ang II infusion

Infusion studies were carried out using Azlet osmotic minipumps (Model 1004). Ang II (BACHEM) dissolved in saline was filled in the minipumps and were prepared to maintain infusion rate of 600 ng/kg/min for 4 weeks. The mice were anesthetized under 2% isoflurane and the minipumps were implanted subcutaneously on the dorsal aspect of the mice.

### Blood pressure recordings

Systolic tail-cuff blood pressure (BP) measurements were carried out using computerized tail-cuff system BP-2000 (Visitech Systems) at the same time of day. Mice were first acclimated to the device by performing 3 days of measurements (20 sequential measurements/day) and then mean blood pressure readings were obtained by averaging 3–5 days of measurements (not inclusive of the 3 acclimation days).

### RNA sequencing

RNA quality was assessed by Agilent BioAnalyzer 2100 by the University of Iowa Institute of Human Genetics, Genomics Division. RNA integrity numbers greater than eight were accepted for RNAseq library preparation. RNA libraries of 150 bp PolyA-enriched RNA were generated, and sequencing was performed on a HiSeq 4000 genome sequencing platform (Illumina). Sequencing results were uploaded and analyzed with BaseSpace (Illumina). Sequences were trimmed to 125 bp using FASTQ

Toolkit (Version 2.2.0) and aligned to *Homo sapiens* HG19 (refseq) using RNA-Seq Alignment (Version 1.1.0). Transcripts were assembled and differential gene expression was determined using Cufflinks Assembly and DE (Version 2.1.0). Ingenuity Pathway Analysis (QIAGEN) was used to analyze significantly regulated genes which were filtered using cutoffs of >1.5 fragments per kilobase per million reads, >1.5-fold changes in gene expression, and a false discovery rate of <0.05. Heatmaps were generated to visualize significantly regulated genes. Data have been deposited in GEO (accession# TBD).

## Metabolic phenotyping

Mice were fasted for 6 hr prior to glucose tolerance tests (GTTs). Baseline glucose levels at 0 min timepoint (fasting glucose) were measured from blood samples collected from tail bleeds using a glucometer (Bayer Healthcare LLC). D-Glucose was injected i.p. (0.75 g/kg body weight) and glucose levels were measured at 7, 15, 30, 60, 90, and 120 min timepoints after injection. For insulin tolerance tests (ITTs), the mice were fasted for 4 hr. Similar to GTTs, the baseline blood glucose levels were measured at 0 min timepoint and 15, 30, 60, 90, and 120 min timepoints post-injection (i.p.) of insulin (HumulinR, 1.25 U/kg body weight). Mouse body composition was performed as previously described (Zhang *et al.*, 2017).

## Statistics

Data are represented as mean  $\pm$  s.e.m. Two-tail unpaired Student's t-tests were used for comparison between two groups. For three or more groups, data were analyzed by one-way analysis of variance (ANOVA) and Tukey's post hoc test. For time-series data in **Figure 5** between two groups, data were analyzed using a two-way ANOVA followed by Bonferroni post hoc test. For GTTs and ITTs, two-way ANOVA was used. A p-value < 0.05 was considered statistically significant. \*, \*\*, and \*\*\* represent a p-value less than 0.05, 0.01, and 0.001, respectively.

## Acknowledgements

RNA-Seq data presented herein were obtained at the Genomics Division of the Iowa Institute of Human Genetics. This work was supported by grants from the NIH/NHLBI R01 HL125436 (CEG), NIH/NHLBI 5R00HL125683, NIH/NIGMS R35 GM137976, Cancer Research Foundation Young Investigator Award (ANS), NIH NIDDK 1R01DK106009, the Roy J Carver Trust (RS), UIHC Center for Hypertension Research Pilot and Feasibility Grant, VA Merit Award I01BX005072 (RS), and King Abdullah International Medical Research Center (KAIMRC) grant RA17-014-A (AA). We thank Dr. Rithwick Rajagopal for insightful reading of the manuscript.

## Additional information

### Funding

Funder	Grant reference number	Author
National Institute of Diabetes and Digestive and Kidney Diseases	R01DK106009	Rajan Sah
National Heart, Lung, and Blood Institute	5R00HL125683	Amber N Stratman
National Heart, Lung, and Blood Institute	R01 HL125436	Chad E Grueter
National Heart, Lung, and Blood Institute	R35 GM137976	Amber N Stratman
VA Merit Award	I01BX005072	Rajan Sah
Cancer Research Foundation	Young Investigator Award	Amber N Stratman
Roy J. Carver Charitable Trust		Rajan Sah
UIHC Center	I01B 005072	Rajan Sah

The funders had no role in study design, data collection and interpretation, or the decision to submit the work for publication.

### Author contributions

Ahmad F Alghanem, Data curation, Software, Formal analysis, Supervision, Validation, Investigation, Visualization, Methodology, Writing - review and editing; Javier Abello, Investigation, Visualization, Methodology; Joshua M Maurer, Chau My Ta, Formal analysis, Investigation, Visualization, Methodology, Writing - review and editing; Ashutosh Kumar, Formal analysis, Supervision, Investigation, Methodology; Susheel K Gunasekar, Formal analysis, Supervision, Investigation, Visualization, Methodology; Urooj Fatima, Oluwaseun Adeola, Formal analysis, Investigation, Methodology; Chen Kang, Formal analysis, Visualization, Methodology; Litao Xie, Robert F Mullins, Amber N Stratman, Supervision, Methodology; Megan Riker, Rachel A Minerath, Methodology; Macaulay Elliot-Hudson, Formal analysis, Methodology; Chad E Grueter, Data curation, Formal analysis, Supervision, Methodology; Rajan Sah, Conceptualization, Data curation, Formal analysis, Supervision, Funding acquisition, Validation, Methodology, Writing - original draft, Project administration, Writing - review and editing

### Author ORCIDs

Ahmad F Alghanem  <https://orcid.org/0000-0002-5823-3806>

Amber N Stratman  <https://orcid.org/0000-0002-8111-4186>

Rajan Sah  <https://orcid.org/0000-0003-1092-1244>

### Ethics

Animal experimentation: This study was performed in accordance with the recommendations in the Guide for the Care and Use of Laboratory Animals of the National Institutes of Health. All of the animals were handled according to the approved Institutional Animal Care and Use Committee (IACUC) protocols of Washington University in St. Louis (20180217) and the University of Iowa (1308148).

### Decision letter and Author response

Decision letter <https://doi.org/10.7554/eLife.61313.sa1>

Author response <https://doi.org/10.7554/eLife.61313.sa2>

## Additional files

### Supplementary files

- Supplementary file 1. RNA sequencing data of human umbilical vein endothelial cell (HUVEC) treated with Ad-shScr and Ad-shLrrc8a.
- Supplementary file 2. Ingenuity pathway analysis.
- Transparent reporting form

### Data availability

RNA sequencing data has been deposited in GEO under accession number GSE166989. All other data available as source data files.

The following dataset was generated:

Author(s)	Year	Dataset title	Dataset URL	Database and Identifier
Alghanem Af, Abello J, Maurer JM, Kumar A, Ta C, Gunasekar SK, Fatima U, Kang C, Xie L, Adeola O, Riker M, Elliott-Hudson M,	2021	The SWELL1-LRRC8 complex regulates endothelial AKT-eNOS- mTOR signaling and vascular function	<a href="https://www.ncbi.nlm.nih.gov/geo/query/acc.cgi?acc=GSE166989">https://www.ncbi.nlm.nih.gov/geo/query/acc.cgi?acc=GSE166989</a>	NCBI Gene Expression Omnibus, GSE166989

Minerath RA,  
Grueter CE, Mullins  
RF, Stratman AN,  
Sah R

## References

- Abascal F, Zardoya R.** 2012. LRRC8 proteins share a common ancestor with pannexins, and may form hexameric channels involved in cell-cell communication. *BioEssays* **34**:551–560. DOI: <https://doi.org/10.1002/bies.201100173>, PMID: 22532330
- Andersson H, Brittebo E.** 2012. Proangiogenic effects of environmentally relevant levels of bisphenol A in human primary endothelial cells. *Archives of Toxicology* **86**:465–474. DOI: <https://doi.org/10.1007/s00204-011-0766-2>, PMID: 22045264
- Arcaro G, Zamboni M, Rossi L, Turcato E, Covi G, Armellini F, Bosello O, Lechi A.** 1999. Body fat distribution predicts the degree of endothelial dysfunction in uncomplicated obesity. *International Journal of Obesity* **23**:936–942. DOI: <https://doi.org/10.1038/sj.jco.0801022>, PMID: 10490799
- Barakat AI, Leaver EV, Pappone PA, Davies PF.** 1999. A flow-activated chloride-selective membrane current in vascular endothelial cells. *Circulation Research* **85**:820–828. DOI: <https://doi.org/10.1161/01.RES.85.9.820>, PMID: 10532950
- Barakat AI.** 1999. Responsiveness of vascular endothelium to shear stress: potential role of ion channels and cellular cytoskeleton (review). *International Journal of Molecular Medicine* **4**:323–332. DOI: <https://doi.org/10.3892/ijmm.4.4.323>, PMID: 10493972
- Brooks SE, Gu X, Samuel S, Marcus DM, Bartoli M, Huang PL, Caldwell RB.** 2001. Reduced severity of oxygen-induced retinopathy in eNOS-deficient mice. *Investigative Ophthalmology & Visual Science* **42**:222–228. PMID: 11133872
- Browe DM, Baumgarten CM.** 2003. Stretch of beta 1 integrin activates an outwardly rectifying chloride current via FAK and src in rabbit ventricular myocytes. *Journal of General Physiology* **122**:689–702. DOI: <https://doi.org/10.1085/jgp.200308899>, PMID: 14610020
- Browe DM, Baumgarten CM.** 2006. EGFR kinase regulates volume-sensitive chloride current elicited by integrin stretch via PI-3K and NADPH oxidase in ventricular myocytes. *Journal of General Physiology* **127**:237–251. DOI: <https://doi.org/10.1085/jgp.200509366>, PMID: 16505146
- Bugiardini R, Manfrini O, Pizzi C, Fontana F, Morgagni G.** 2004. Endothelial function predicts future development of coronary artery disease: a study of women with chest pain and normal coronary angiograms. *Circulation* **109**:2518–2523. DOI: <https://doi.org/10.1161/01.CIR.0000128208.22378.E3>, PMID: 15136498
- Cahill PA, Redmond EM.** 2016. Vascular endothelium - Gatekeeper of vessel health. *Atherosclerosis* **248**:97–109. DOI: <https://doi.org/10.1016/j.atherosclerosis.2016.03.007>, PMID: 26994427
- Cappelli HC, Kanugula AK, Adapala RK, Amin V, Sharma P, Midha P, Paruchuri S, Thodeti CK.** 2019. Mechanosensitive TRPV4 channels stabilize VE-cadherin junctions to regulate tumor vascular integrity and metastasis. *Cancer Letters* **442**:15–20. DOI: <https://doi.org/10.1016/j.canlet.2018.07.042>, PMID: 30401632
- Clapp BR, Hingorani AD, Kharbanda RK, Mohamed-Ali V, Stephens JW, Vallance P, MacAllister RJ.** 2004. Inflammation-induced endothelial dysfunction involves reduced nitric oxide bioavailability and increased oxidant stress. *Cardiovascular Research* **64**:172–178. DOI: <https://doi.org/10.1016/j.cardiores.2004.06.020>, PMID: 15364625
- Coste B, Mathur J, Schmidt M, Earley TJ, Ranade S, Petrus MJ, Dubin AE, Patapoutian A.** 2010. Piezo1 and Piezo2 are essential components of distinct mechanically activated cation channels. *Science* **330**:55–60. DOI: <https://doi.org/10.1126/science.1193270>, PMID: 20813920
- Coste B, Xiao B, Santos JS, Syeda R, Grandl J, Spencer KS, Kim SE, Schmidt M, Mathur J, Dubin AE, Montal M, Patapoutian A.** 2012. Piezo proteins are pore-forming subunits of mechanically activated channels. *Nature* **483**:176–181. DOI: <https://doi.org/10.1038/nature10812>, PMID: 22343900
- Dalsgaard T, Sonkusare SK, Teuscher C, Poynter ME, Nelson MT.** 2016. Pharmacological inhibitors of TRPV4 channels reduce cytokine production, restore endothelial function and increase survival in septic mice. *Scientific Reports* **6**:33841. DOI: <https://doi.org/10.1038/srep33841>, PMID: 27653046
- Ding Y, Shan L, Nai W, Lin X, Zhou L, Dong X, Wu H, Xiao M, Zhou X, Wang L, Li T, Fu Y, Lin Y, Jia C, Dai M, Bai X.** 2018. DEPTOR Deficiency-Mediated mTORc1 hyperactivation in vascular endothelial cells promotes angiogenesis. *Cellular Physiology and Biochemistry* **46**:520–531. DOI: <https://doi.org/10.1159/000488619>, PMID: 29614494
- Duncan ER, Crossey PA, Walker S, Anilkumar N, Poston L, Douglas G, Ezzat VA, Wheatcroft SB, Shah AM, Kearney MT, Kearney MI.** 2008. Effect of endothelium-specific insulin resistance on endothelial function in vivo. *Diabetes* **57**:3307–3314. DOI: <https://doi.org/10.2337/db07-1111>, PMID: 18835939
- Dunn KM, Hill-Eubanks DC, Liedtke WB, Nelson MT.** 2013. TRPV4 channels stimulate Ca<sup>2+</sup>-induced Ca<sup>2+</sup> release in astrocytic endfeet and amplify neurovascular coupling responses. *PNAS* **110**:6157–6162. DOI: <https://doi.org/10.1073/pnas.1216514110>, PMID: 23530219
- Earley S, Heppner TJ, Nelson MT, Brayden JE.** 2005. TRPV4 forms a novel Ca<sup>2+</sup> signaling complex with ryanodine receptors and BKCa channels. *Circulation Research* **97**:1270–1279. DOI: <https://doi.org/10.1161/01.RES.0000194321.60300.d6>, PMID: 16269659

- Earley S**, Pauyo T, Drapp R, Tavares MJ, Liedtke W, Brayden JE. 2009. TRPV4-dependent dilation of peripheral resistance arteries influences arterial pressure. *American Journal of Physiology-Heart and Circulatory Physiology* **297**:H1096–H1102. DOI: <https://doi.org/10.1152/ajpheart.00241.2009>, PMID: 19617407
- Egorov YV**, Lang D, Tyan L, Turner D, Lim E, Piro ZD, Hernandez JJ, Lodin R, Wang R, Schmuck EG, Raval AN, Ralphe CJ, Kamp TJ, Rosenshtraukh LV, Glukhov AV. 2019. Caveolae-Mediated activation of mechanosensitive chloride channels in pulmonary veins triggers atrial arrhythmogenesis. *Journal of the American Heart Association* **8**:e012748. DOI: <https://doi.org/10.1161/JAHA.119.012748>, PMID: 31597508
- Feng Y**, Venema VJ, Venema RC, Tsai N, Caldwell RB. 1999. VEGF induces nuclear translocation of Flk-1/KDR, endothelial nitric oxide synthase, and caveolin-1 in vascular endothelial cells. *Biochemical and Biophysical Research Communications* **256**:192–197. DOI: <https://doi.org/10.1006/bbrc.1998.9790>, PMID: 10066445
- Fulton D**, Fontana J, Sowa G, Gratton J-P, Lin M, Li K-X, Michell B, Kemp BE, Rodman D, Sessa WC. 2002. Localization of endothelial Nitric-oxide synthase phosphorylated on serine 1179 and nitric oxide in golgi and plasma membrane defines the existence of two pools of active enzyme. *Journal of Biological Chemistry* **277**:4277–4284. DOI: <https://doi.org/10.1074/jbc.M106302200>
- Gerhold KA**, Schwartz MA. 2016. Ion channels in endothelial responses to fluid shear stress. *Physiology* **31**:359–369. DOI: <https://doi.org/10.1152/physiol.00007.2016>, PMID: 27511462
- Gobeil F**, Zhu T, Brault S, Geha A, Vazquez-Tello A, Fortier A, Barbaz D, Checchin D, Hou X, Nader M, Bkaily G, Gratton JP, Heveker N, Ribeiro-da-Silva A, Peri K, Bard H, Chorvatova A, D'Orléans-Juste P, Goetzl EJ, Chemtob S. 2006. Nitric oxide signaling via nuclearized endothelial nitric-oxide synthase modulates expression of the immediate early genes iNOS and mPGES-1. *Journal of Biological Chemistry* **281**:16058–16067. DOI: <https://doi.org/10.1074/jbc.M602219200>, PMID: 16574649
- Goettsch C**, Goettsch W, Arsov A, Hofbauer LC, Bornstein SR, Morawietz H. 2009. Long-term cyclic strain downregulates endothelial Nox4. *Antioxidants & Redox Signaling* **11**:2385–2397. DOI: <https://doi.org/10.1089/ars.2009.2561>, PMID: 19309265
- Goligorsky MS**, Li H, Brodsky S, Chen J. 2002. Relationships between caveolae and eNOS: everything in proximity and the proximity of everything. *American Journal of Physiology-Renal Physiology* **283**:F1–F10. DOI: <https://doi.org/10.1152/ajprenal.00377.2001>, PMID: 12060581
- Gunasekar SK**, Xie L, Sah R. 2019. SWELL signalling in adipocytes: can fat 'feel' fat? *Adipocyte* **8**:223–228. DOI: <https://doi.org/10.1080/21623945.2019.1612223>, PMID: 31112068
- Harb D**, Bujold K, Febbraio M, Sirois MG, Ong H, Marleau S. 2009. The role of the scavenger receptor CD36 in regulating mononuclear phagocyte trafficking to atherosclerotic lesions and vascular inflammation. *Cardiovascular Research* **83**:42–51. DOI: <https://doi.org/10.1093/cvr/cvp081>, PMID: 19264766
- Harratz OF**, Longden TA, Hill-Eubanks D, Nelson MT. 2018. PIP2 depletion promotes TRPV4 channel activity in mouse brain capillary endothelial cells. *eLife* **7**:e38689. DOI: <https://doi.org/10.7554/eLife.38689>, PMID: 30084828
- Hsu HJ**, Lee CF, Locke A, Vanderzyl SQ, Kaunas R. 2010. Stretch-induced stress fiber remodeling and the activations of JNK and ERK depend on mechanical strain rate, but not FAK. *PLOS ONE* **5**:e12470. DOI: <https://doi.org/10.1371/journal.pone.0012470>, PMID: 20814573
- Hu Z**, Xiong Y, Han X, Geng C, Jiang B, Huo Y, Luo J. 2013. Acute mechanical stretch promotes eNOS activation in venous endothelial cells mainly via PKA and akt pathways. *PLOS ONE* **8**:e71359. DOI: <https://doi.org/10.1371/journal.pone.0071359>, PMID: 23977025
- Janus A**, Szahidewicz-Krupska E, Mazur G, Doroszko A. 2016. Insulin resistance and endothelial dysfunction constitute a common therapeutic target in cardiometabolic disorders. *Mediators of Inflammation* **2016**:1–10. DOI: <https://doi.org/10.1155/2016/3634948>
- Ju H**, Zou R, Venema VJ, Venema RC. 1997. Direct interaction of endothelial nitric-oxide synthase and caveolin-1 inhibits synthase activity. *Journal of Biological Chemistry* **272**:18522–18525. DOI: <https://doi.org/10.1074/jbc.272.30.18522>, PMID: 9228013
- Jufri NF**, Mohamedali A, Avolio A, Baker MS. 2015. Mechanical stretch: physiological and pathological implications for human vascular endothelial cells. *Vascular Cell* **7**:8. DOI: <https://doi.org/10.1186/s13221-015-0033-z>, PMID: 26388991
- Kang C**, Xie L, Gunasekar SK, Mishra A, Zhang Y, Pai S, Gao Y, Kumar A, Norris AW, Stephens SB, Sah R. 2018. SWELL1 is a glucose sensor regulating  $\beta$ -cell excitability and systemic glycaemia. *Nature Communications* **9**:367. DOI: <https://doi.org/10.1038/s41467-017-02664-0>, PMID: 29371604
- Kataoka C**, Egashira K, Inoue S, Takemoto M, Ni W, Koyanagi M, Kitamoto S, Usui M, Kaibuchi K, Shimokawa H, Takeshita A. 2002. Important role of Rho-kinase in the pathogenesis of cardiovascular inflammation and remodeling induced by long-term blockade of nitric oxide synthesis in rats. *Hypertension* **39**:245–250. DOI: <https://doi.org/10.1161/hy0202.103271>, PMID: 11847192
- Kearney MT**, Duncan ER, Kahn M, Wheatcroft SB. 2008. Insulin resistance and endothelial cell dysfunction: studies in mammalian models. *Experimental Physiology* **93**:158–163. DOI: <https://doi.org/10.1113/expphysiol.2007.039172>, PMID: 17933859
- Kennedy DJ**, Kuchibhotla SD, Guy E, Park YM, Nimako G, Vanegas D, Morton RE, Febbraio M. 2009. Dietary cholesterol plays a role in CD36-mediated atherogenesis in LDLR-knockout mice. *Arteriosclerosis, Thrombosis, and Vascular Biology* **29**:1481–1487. DOI: <https://doi.org/10.1161/ATVBAHA.109.191940>, PMID: 19608973
- Koh W**, Stratman AN, Sacharidou A, Davis GE. 2008. In vitro three dimensional collagen matrix models of endothelial lumen formation during vasculogenesis and angiogenesis. *Methods in Enzymology* **443**:83–101. DOI: [https://doi.org/10.1016/S0076-6879\(08\)02005-3](https://doi.org/10.1016/S0076-6879(08)02005-3), PMID: 18772012

- Kondo T**, Vicent D, Suzuma K, Yanagisawa M, King GL, Holzenberger M, Kahn CR. 2003. Knockout of insulin and IGF-1 receptors on vascular endothelial cells protects against retinal neovascularization. *Journal of Clinical Investigation* **111**:1835–1842. DOI: <https://doi.org/10.1172/JCI200317455>, PMID: 12813019
- Kubota K**, Kim JY, Sawada A, Tokimasa S, Fujisaki H, Matsuda-Hashii Y, Ozono K, Hara J. 2004. LRR8 involved in B cell development belongs to a novel family of leucine-rich repeat proteins. *FEBS Letters* **564**:147–152. DOI: [https://doi.org/10.1016/S0014-5793\(04\)00332-1](https://doi.org/10.1016/S0014-5793(04)00332-1), PMID: 15094057
- Kumar L**, Chou J, Yee CS, Borzutzky A, Vollmann EH, von Andrian UH, Park SY, Hollander G, Manis JP, Poliani PL, Geha RS. 2014. Leucine-rich repeat containing 8A (LRR8A) is essential for T lymphocyte development and function. *Journal of Experimental Medicine* **211**:929–942. DOI: <https://doi.org/10.1084/jem.20131379>, PMID: 24752297
- Kumar A**, Xie L, Ta CM, Hinton AO, Gunasekar SK, Minerath RA, Shen K, Maurer JM, Grueter CE, Abel ED, Meyer G, Sah R. 2020. SWELL1 regulates skeletal muscle cell size, intracellular signaling, adiposity and glucose metabolism. *eLife* **9**:e58941. DOI: <https://doi.org/10.7554/eLife.58941>, PMID: 32930093
- Li J**, Hou B, Tumova S, Muraki K, Bruns A, Ludlow MJ, Sedo A, Hyman AJ, McKeown L, Young RS, Yuldasheva NY, Majeed Y, Wilson LA, Rode B, Bailey MA, Kim HR, Fu Z, Carter DA, Bilton J, Imrie H, et al. 2014. Piezo1 integration of vascular architecture with physiological force. *Nature* **515**:279–282. DOI: <https://doi.org/10.1038/nature13701>, PMID: 25119035
- Liu XM**, Ensenat D, Wang H, Schafer AI, Durante W. 2003. Physiologic cyclic stretch inhibits apoptosis in vascular endothelium. *FEBS Letters* **541**:52–56. DOI: [https://doi.org/10.1016/S0014-5793\(03\)00285-0](https://doi.org/10.1016/S0014-5793(03)00285-0), PMID: 12706818
- Lück JC**, Puchkov D, Ullrich F, Jentsch TJ. 2018. LRR8/VRAC anion channels are required for late stages of spermatid development in mice. *Journal of Biological Chemistry* **293**:11796–11808. DOI: <https://doi.org/10.1074/jbc.RA118.003853>, PMID: 29880644
- Mendoza SA**, Fang J, Gutterman DD, Wilcox DA, Bubolz AH, Li R, Suzuki M, Zhang DX. 2010. TRPV4-mediated endothelial Ca<sup>2+</sup> influx and vasodilation in response to shear stress. *American Journal of Physiology. Heart and Circulatory Physiology* **298**:466–476. DOI: <https://doi.org/10.1152/ajpheart.00854.2009>, PMID: 19966050
- Mercado J**, Baylie R, Navedo MF, Yuan C, Scott JD, Nelson MT, Brayden JE, Santana LF. 2014. Local control of TRPV4 channels by AKAP150-targeted PKC in arterial smooth muscle. *Journal of General Physiology* **143**:559–575. DOI: <https://doi.org/10.1085/jgp.201311050>, PMID: 24778429
- Montagnani M**, Ravichandran LV, Chen H, Esposito DL, Quon MJ. 2002. Insulin receptor substrate-1 and phosphoinositide-dependent kinase-1 are required for insulin-stimulated production of nitric oxide in endothelial cells. *Molecular Endocrinology* **16**:1931–1942. DOI: <https://doi.org/10.1210/me.2002-0074>, PMID: 12145346
- Morello F**, Perino A, Hirsch E. 2009. Phosphoinositide 3-kinase signalling in the vascular system. *Cardiovascular Research* **82**:261–271. DOI: <https://doi.org/10.1093/cvr/cvn325>, PMID: 19038971
- Muniyappa R**, Sowers JR. 2013. Role of insulin resistance in endothelial dysfunction. *Reviews in Endocrine and Metabolic Disorders* **14**:5–12. DOI: <https://doi.org/10.1007/s11154-012-9229-1>, PMID: 23306778
- Murphy C**, Kanaganayagam GS, Jiang B, Chowienczyk PJ, Zbinden R, Saha M, Rahman S, Shah AM, Marber MS, Kearney MT. 2007. Vascular dysfunction and reduced circulating endothelial progenitor cells in young healthy UK south asian men. *Arteriosclerosis, Thrombosis, and Vascular Biology* **27**:936–942. DOI: <https://doi.org/10.1161/01.ATV.0000258788.11372.d0>, PMID: 17255539
- Nakao M**, Ono K, Fujisawa S, Iijima T. 1999. Mechanical stress-induced Ca<sup>2+</sup> entry and Cl<sup>-</sup> current in cultured human aortic endothelial cells. *The American Journal of Physiology* **276**:238–249. DOI: <https://doi.org/10.1152/ajpcell.1999.276.1.C238>, PMID: 9886940
- Nassoy P**, Lamaze C. 2012. Stressing caveolae new role in cell mechanics. *Trends in Cell Biology* **22**:381–389. DOI: <https://doi.org/10.1016/j.tcb.2012.04.007>, PMID: 22613354
- Nilius B**, Droogmans G. 2001. Ion channels and their functional role in vascular endothelium. *Physiological Reviews* **81**:1415–1459. DOI: <https://doi.org/10.1152/physrev.2001.81.4.1415>, PMID: 11581493
- Palmer RM**, Ferrige AG, Moncada S. 1987. Nitric oxide release accounts for the biological activity of endothelium-derived relaxing factor. *Nature* **327**:524–526. DOI: <https://doi.org/10.1038/327524a0>, PMID: 3495737
- Park YM**. 2014. CD36, a scavenger receptor implicated in atherosclerosis. *Experimental & Molecular Medicine* **46**:e99. DOI: <https://doi.org/10.1038/emm.2014.38>, PMID: 24903227
- Qiu Z**, Dubin AE, Mathur J, Tu B, Reddy K, Miraglia LJ, Reinhardt J, Orth AP, Patapoutian A. 2014. SWELL1, a plasma membrane protein, is an essential component of volume-regulated anion channel. *Cell* **157**:447–458. DOI: <https://doi.org/10.1016/j.cell.2014.03.024>, PMID: 24725410
- Quillon A**, Fromy B, Debret R. 2015. Endothelium microenvironment sensing leading to nitric oxide mediated vasodilation: a review of nervous and biomechanical signals. *Nitric Oxide* **45**:20–26. DOI: <https://doi.org/10.1016/j.niox.2015.01.006>, PMID: 25638487
- Radomski MW**, Palmer RM, Moncada S. 1987a. The role of nitric oxide and cGMP in platelet adhesion to vascular endothelium. *Biochemical and Biophysical Research Communications* **148**:1482–1489. DOI: [https://doi.org/10.1016/S0006-291X\(87\)80299-1](https://doi.org/10.1016/S0006-291X(87)80299-1), PMID: 2825688
- Radomski MW**, Palmer RM, Moncada S. 1987b. Endogenous nitric oxide inhibits human platelet adhesion to vascular endothelium. *The Lancet* **2**:1057–1058. DOI: [https://doi.org/10.1016/S0140-6736\(87\)91481-4](https://doi.org/10.1016/S0140-6736(87)91481-4), PMID: 2889967
- Rode B**, Shi J, Endesh N, Drinkhill MJ, Webster PJ, Lotteau SJ, Bailey MA, Yuldasheva NY, Ludlow MJ, Cubbon RM, Li J, Futers TS, Morley L, Gaunt HJ, Marszalek K, Viswambaran H, Cuthbertson K, Baxter PD, Foster R, Sukumar P, et al. 2017. Piezo1 channels sense whole body physical activity to reset cardiovascular homeostasis

- and enhance performance. *Nature Communications* **8**:350. DOI: <https://doi.org/10.1038/s41467-017-00429-3>, PMID: 28839146
- Romanenko VG**, Davies PF, Levitan I. 2002. Dual effect of fluid shear stress on volume-regulated anion current in bovine aortic endothelial cells. *American Journal of Physiology-Cell Physiology* **282**:C708–C718. DOI: <https://doi.org/10.1152/ajpcell.00247.2001>, PMID: 11880259
- Salameh A**, Galvagni F, Bardelli M, Bussolino F, Oliviero S. 2005. Direct recruitment of CRK and GRB2 to VEGFR-3 induces proliferation, migration, and survival of endothelial cells through the activation of ERK, AKT, and JNK pathways. *Blood* **106**:3423–3431. DOI: <https://doi.org/10.1182/blood-2005-04-1388>, PMID: 16076871
- Sawada A**, Takihara Y, Kim JY, Matsuda-Hashii Y, Tokimasa S, Fujisaki H, Kubota K, Endo H, Onodera T, Ohta H, Ozono K, Hara J. 2003. A congenital mutation of the novel gene LRRC8 causes agammaglobulinemia in humans. *Journal of Clinical Investigation* **112**:1707–1713. DOI: <https://doi.org/10.1172/JCI18937>, PMID: 14660746
- Schächinger V**, Britten MB, Zeiher AM. 2000. Prognostic impact of coronary vasodilator dysfunction on adverse long-term outcome of coronary heart disease. *Circulation* **101**:1899–1906. DOI: <https://doi.org/10.1161/01.CIR.101.16.1899>, PMID: 10779454
- Schäfer A**, Widder J, Eigenthaler M, Ertl G, Bauersachs J. 2004a. Reduced basal nitric oxide bioavailability and platelet activation in young spontaneously hypertensive rats. *Biochemical Pharmacology* **67**:2273–2279. DOI: <https://doi.org/10.1016/j.bcp.2004.02.034>, PMID: 15163558
- Schäfer A**, Wiesmann F, Neubauer S, Eigenthaler M, Bauersachs J, Channon KM. 2004b. Rapid regulation of platelet activation in vivo by nitric oxide. *Circulation* **109**:1819–1822. DOI: <https://doi.org/10.1161/01.CIR.0000126837.88743.DD>, PMID: 15066953
- Schindelin J**, Arganda-Carreras I, Frise E, Kaynig V, Longair M, Pietzsch T, Preibisch S, Rueden C, Saalfeld S, Schmid B, Tinevez JY, White DJ, Hartenstein V, Eliceiri K, Tomancak P, Cardona A. 2012. Fiji: an open-source platform for biological-image analysis. *Nature Methods* **9**:676–682. DOI: <https://doi.org/10.1038/nmeth.2019>, PMID: 22743772
- Sedding DG**, Hermsen J, Seay U, Eickelberg O, Kummer W, Schwencke C, Strasser RH, Tillmanns H, Braun-Dullaes RC. 2005. Caveolin-1 facilitates mechanosensitive protein kinase B (Akt) signaling in vitro and in vivo. *Circulation Research* **96**:635–642. DOI: <https://doi.org/10.1161/01.RES.0000160610.61306.0f>, PMID: 15731459
- Shi F**, Chiu YJ, Cho Y, Bullard TA, Sokabe M, Fujiwara K. 2007. Down-regulation of ERK but not MEK phosphorylation in cultured endothelial cells by repeated changes in cyclic stretch. *Cardiovascular Research* **73**:813–822. DOI: <https://doi.org/10.1016/j.cardiores.2006.12.014>, PMID: 17289004
- Silverstein RL**, Febbraio M. 2009. CD36, a scavenger receptor involved in immunity, metabolism, angiogenesis, and behavior. *Science Signaling* **2**:re3. DOI: <https://doi.org/10.1126/scisignal.272re3>, PMID: 19471024
- Sinha B**, Köster D, Ruez R, Gonnord P, Bastiani M, Abankwa D, Stan RV, Butler-Browne G, Védie B, Johannes L, Morone N, Parton RG, Raposo G, Sens P, Lamaze C, Nassoy P. 2011. Cells respond to mechanical stress by rapid disassembly of caveolae. *Cell* **144**:402–413. DOI: <https://doi.org/10.1016/j.cell.2010.12.031>, PMID: 21295700
- Sonkusare SK**, Bonev AD, Ledoux J, Liedtke W, Kotlikoff MI, Heppner TJ, Hill-Eubanks DC, Nelson MT. 2012. Elementary Ca<sup>2+</sup> signals through endothelial TRPV4 channels regulate vascular function. *Science* **336**:597–601. DOI: <https://doi.org/10.1126/science.1216283>, PMID: 22556255
- Sonkusare SK**, Dalsgaard T, Bonev AD, Hill-Eubanks DC, Kotlikoff MI, Scott JD, Santana LF, Nelson MT. 2014. AKAP150-dependent cooperative TRPV4 channel gating is central to endothelium-dependent vasodilation and is disrupted in hypertension. *Science Signaling* **7**:ra66. DOI: <https://doi.org/10.1126/scisignal.2005052>, PMID: 25005230
- Steinberg HO**, Chaker H, Leaming R, Johnson A, Brechtel G, Baron AD. 1996. Obesity/insulin resistance is associated with endothelial dysfunction. Implications for the syndrome of insulin resistance. *Journal of Clinical Investigation* **97**:2601–2610. DOI: <https://doi.org/10.1172/JCI118709>, PMID: 8647954
- Stuhlmann T**, Planells-Cases R, Jentsch TJ. 2018. LRRC8/VRAC anion channels enhance  $\beta$ -cell glucose sensing and insulin secretion. *Nature Communications* **9**:1974. DOI: <https://doi.org/10.1038/s41467-018-04353-y>, PMID: 29773801
- Syeda R**, Qiu Z, Dubin AE, Murthy SE, Florendo MN, Mason DE, Mathur J, Cahalan SM, Peters EC, Montal M, Patapoutian A. 2016. LRRC8 proteins form Volume-Regulated anion channels that sense ionic strength. *Cell* **164**:499–511. DOI: <https://doi.org/10.1016/j.cell.2015.12.031>, PMID: 26824658
- Tack CJ**, Ong MK, Lutterman JA, Smits P. 1998. Insulin-induced vasodilatation and endothelial function in obesity/insulin resistance. Effects of troglitazone. *Diabetologia* **41**:569–576. DOI: <https://doi.org/10.1007/s001250050948>, PMID: 9628275
- Trouet D**, Nilius B, Jacobs A, Remacle C, Droogmans G, Eggermont J. 1999. Caveolin-1 modulates the activity of the volume-regulated chloride channel. *The Journal of Physiology* **520 Pt 1**:113–119. DOI: <https://doi.org/10.1111/j.1469-7793.1999.t01-1-00113.x>, PMID: 10517805
- Trouet D**, Hermans D, Droogmans G, Nilius B, Eggermont J. 2001. Inhibition of volume-regulated anion channels by dominant-negative caveolin-1. *Biochemical and Biophysical Research Communications* **284**:461–465. DOI: <https://doi.org/10.1006/bbrc.2001.4995>, PMID: 11394902
- Venema VJ**, Zou R, Ju H, Marrero MB, Venema RC. 1997. Caveolin-1 detergent solubility and association with endothelial nitric oxide synthase is modulated by tyrosine phosphorylation. *Biochemical and Biophysical Research Communications* **236**:155–161. DOI: <https://doi.org/10.1006/bbrc.1997.6921>, PMID: 9223444

- Voss FK**, Ullrich F, Münch J, Lazarow K, Lutter D, Mah N, Andrade-Navarro MA, von Kries JP, Stauber T, Jentsch TJ. 2014. Identification of LRRC8 heteromers as an essential component of the volume-regulated anion channel VRAC. *Science* **344**:634–638. DOI: <https://doi.org/10.1126/science.1252826>, PMID: 24790029
- Wang R**, Lu Y, Gunasekar S, Zhang Y, Benson CJ, Chapleau MW, Sah R, Abboud FM. 2017. The volume-regulated anion channel (LRRC8) in nodose neurons is sensitive to acidic pH. *JCI Insight* **2**:e90632. DOI: <https://doi.org/10.1172/jci.insight.90632>, PMID: 28289711
- Wang W**, Wang D, Kong C, Li S, Xie L, Lin Z, Zheng Y, Zhou J, Han Y, Ji Y. 2019. eNOS S-nitrosylation mediated OxLDL-induced endothelial dysfunction via increasing the interaction of eNOS with  $\beta$ -catenin. *Biochimica Et Biophysica Acta (BBA) - Molecular Basis of Disease* **1865**:1793–1801. DOI: <https://doi.org/10.1016/j.bbadis.2018.02.009>, PMID: 29471036
- Westerbacka J**, Vehkavaara S, Bergholm R, Wilkinson I, Cockcroft J, Yki-Järvinen H. 1999. Marked resistance of the ability of insulin to decrease arterial stiffness characterizes human obesity. *Diabetes* **48**:821–827. DOI: <https://doi.org/10.2337/diabetes.48.4.821>, PMID: 10102699
- Williams IL**, Chowienczyk PJ, Wheatcroft SB, Patel A, Sherwood R, Momin A, Shah AM, Kearney MT. 2006. Effect of fat distribution on endothelial-dependent and endothelial-independent vasodilatation in healthy humans. *Diabetes, Obesity and Metabolism* **8**:296–301. DOI: <https://doi.org/10.1111/j.1463-1326.2005.00505.x>, PMID: 16634989
- Wu KK**. 2002. Regulation of endothelial nitric oxide synthase activity and gene expression. *Annals of the New York Academy of Sciences* **962**:122–130. DOI: <https://doi.org/10.1111/j.1749-6632.2002.tb04062.x>, PMID: 12076969
- Xie L**, Zhang Y, Gunasekar SK, Mishra A, Cao L, Sah R. 2017. Induction of adipose and hepatic SWELL1 expression is required for maintaining systemic insulin-sensitivity in obesity. *Channels* **11**:673–677. DOI: <https://doi.org/10.1080/19336950.2017.1373225>, PMID: 28873008
- Zeng G**, Nystrom FH, Ravichandran LV, Cong LN, Kirby M, Mostowski H, Quon MJ. 2000. Roles for insulin receptor, PI3-kinase, and akt in insulin-signaling pathways related to production of nitric oxide in human vascular endothelial cells. *Circulation* **101**:1539–1545. DOI: <https://doi.org/10.1161/01.CIR.101.13.1539>, PMID: 10747347
- Zeng G**, Quon MJ. 1996. Insulin-stimulated production of nitric oxide is inhibited by wortmannin. Direct measurement in vascular endothelial cells. *Journal of Clinical Investigation* **98**:894–898. DOI: <https://doi.org/10.1172/JCI118871>, PMID: 8770859
- Zhang DX**, Mendoza SA, Bubolz AH, Mizuno A, Ge ZD, Li R, Warltier DC, Suzuki M, Gutterman DD. 2009. Transient receptor potential vanilloid type 4-deficient mice exhibit impaired endothelium-dependent relaxation induced by acetylcholine in vitro and in vivo. *Hypertension* **53**:532–538. DOI: <https://doi.org/10.1161/HYPERTENSIONAHA.108.127100>, PMID: 19188524
- Zhang Y**, Xie L, Gunasekar SK, Tong D, Mishra A, Gibson WJ, Wang C, Fidler T, Marthaler B, Klingelhutz A, Abel ED, Samuel I, Smith JK, Cao L, Sah R. 2017. SWELL1 is a regulator of adipocyte size, insulin signalling and glucose homeostasis. *Nature Cell Biology* **19**:504–517. DOI: <https://doi.org/10.1038/ncb3514>, PMID: 28436964
- Zhao J**, Wang W, Ha CH, Kim JY, Wong C, Redmond EM, Hamik A, Jain MK, Feng GS, Jin ZG. 2011. Endothelial Grb2-associated binder 1 is crucial for postnatal angiogenesis. *Arteriosclerosis, Thrombosis, and Vascular Biology* **31**:1016–1023. DOI: <https://doi.org/10.1161/ATVBAHA.111.224493>, PMID: 21372298